Addis Ababa University
School of Graduate Studies
Department of Earth Sciences

INTEGRATED GEOPHYSICAL INVESTIGATION FOR ENGINEERING SITE CHARACTERIZATIONS OF DAM CONSTRUCTION SITE, NEAR WUKRO TOWN, TIGRAY, NORTHERN ETHIOPIA

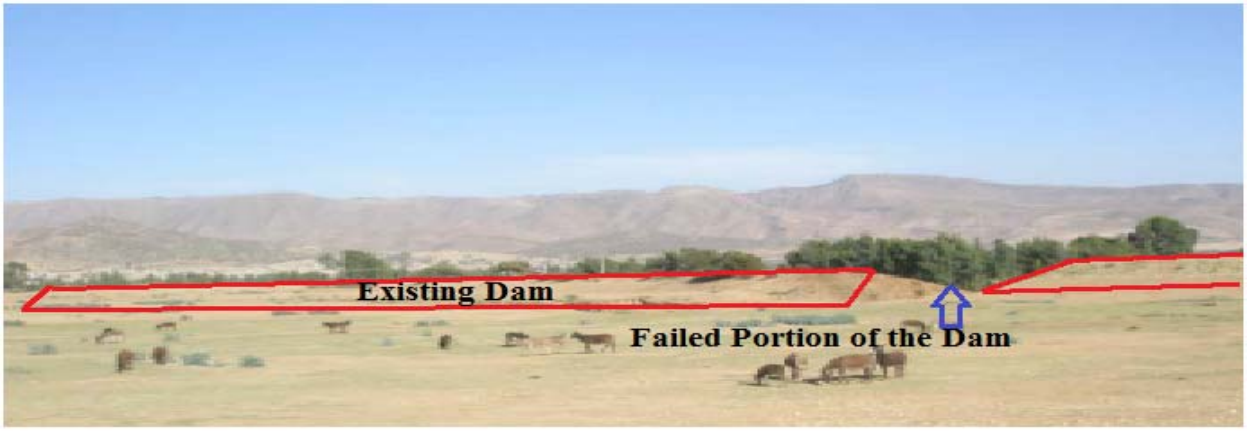

By: Solomun Atsbaha

A THESIS SUBMITTED TO THE SCHOOL OF GRADUATE STUDIES OF ADDIS ABABA UNIVERSITY IN PARTIAL FULFILLMENT OF THE REQUIREMENTS FOR THE DEGREE OF MASTER OF SCIENCE (MSc) IN GEOPHYSICS

June, 2012

Addis Ababa University
School of Graduate Studies
Department of Earth Sciences

INTEGRATED GEOPHYSICAL INVESTIGATION FOR ENGINEERING SITE CHARACTERIZATIONS OF DAM CONSTRUCTION SITE, NEAR WUKRO TOWN, TIGRAY, NORTHERN ETHIOPIA

By

Solomun Atsbaha

Faculty of Science

Department of Earth Science

Approved by board of examiners:-

Dr. Seifu Kebede Signature _____

Chairman, Department of Earth Science

Dr. Tigstu Haile Signature _____

Advisor

Dr. Tilahun Mammo Signature _____

Advisor

Dr. Asfawossen Assrat Signature _____

Internal Examiner

Dr. Girma W/tenisae Signature _____

External Examiner

Abstract

Integrated geophysical investigations using 2D electrical imaging, vertical electrical sounding and magnetic methods have been conducted for engineering site characterization of a dam foundation located at Hizaeti Afras near Wukro town, Tigray Regional State, North Ethiopia. The main objective of the study was to examine the suitability of the subsurface geological formations and structures for foundation of the proposed dam project.

From the results of the survey, it has been possible to map the stratification of the subsurface layers, their vertical and lateral extent, and hence the depth to the sound bedrock suitable for dam foundation is determined. It has also been possible to map areas of weakness in the subsurface that could be detrimental to the life of the dam.

According to the interpretation of the geophysical results, the near surface geology of the study area includes three layers. The first layer which is the top soil has considerably varying thickness (2m-9m) over the area. The second layer is interpreted as a weathered and fractured limestone with shale intercalation. And it extends to depth of about 27m on the western and 33m on the northern part of the survey area. However, its depth extent on the eastern and southern part is about 17m to 21m. The third layer which is characterized by higher apparent resistivity response is interpreted as black limestone which could be considered as the bed rock in the area. This layer has undulating nature and the depth to this bed rock surface is deeper in the western and northern portions and become shallow towards the eastern and southern portions of the survey area.

Based on the pseudo-depth and sliced-stacked depth maps the study area can be divided in to three distinct zones. The first zone which is characterized by very low apparent resistivity values includes the western and northeastern portions of the study area. This is interpreted to be the response of the water saturated weathered and fractured limestone. The second zone that exhibits intermediate apparent resistivity values comprises of the central part of the study area with a narrow strip in the central-east. This area is interpreted to be covered by weathered and fractured limestone with shale intercalation. The third zone which is characterized by very high apparent resistivity response comprises of the southeastern part of the area and it is interpreted as a black limestone formation.

From a combined interpretation of the geophysical data, four weak zones have been identified over the survey area which are oriented in N-S, NE-SW, NW-SE and E-W direction. The N-S running major weak zone is in the region (about 100m -110m from the western side of the dam axis) where an earlier dam built on the site has broken through.

As a further conclusion from the work, it is suggested that the dam axis has to be relocated towards the downstream side by about 150m from the intended location. This relocated dam axis will get the sound foundation at shallower depth and has a reduced risk from the weak zones trending NE-SW and NW-SE. In addition special attention should be given to the western and northeastern part of the study area and the weak zones in designing and implementation of the dam foundation.

Acknowledgement

First of all I would like to thank my advisors Dr. Tigistu Haile and Dr. Tilahun mammo for their constructive comments and suggestions throughout the research work.

I do not have words to thank my sister Medhin Teklay. Medu this is all yours so thank very much.

I feel greatfull to thank my brother Atakilti Getachew too for his continuous support during my stay in school.

I am also thankful to St'mary college for all their support during the field work. thank you aba Melaku.

My mother, sister (Mulu) and all my brothers, specially Mihreteab, Asmelash, Gebru and Kidat thank you all.

Oh friends, Alemayohu, Mohamed, Teshale, Yonnas, and Kunom I did not forgot you, it gives me pleasure to thank you.

Last but not least, my beloved wife and son thank you for all what you did to me. I do not have words that can explain my feelings for you so thank you again.

Table of contents

Chapter - 2

Chapter - 3

Chapter - 5

Chapter - 6

List of Figures

List of Tables

List of Appendices

Acronym

CST	Constant Separation Traversing
D/s	Downstream
ERT	Electrical Resistivity Tomography
ETB	Ethiopian Birr
Fig	Figure
G.C	Gregorian calendar
GPS	Global Positioning System
Ha	Hectars
IGRF	International Geomagnetic Reference Field
TWMEB	Tigray Water resource, Mines and Energy Bureau
NE	Northeast
NW	Northwest
RMS	Root Mean Square Error
RTP	Reduction to the Pole
SE	Southeast
SW	Southwest
U.S	United States of America
U/s	Upstream
UTM	Universal Transversal Mercator
VES	Vertical Electrical Sounding
2D	Two Dimensional

CHAPTER - 1

INTRODUCTION

1.1 General

The purpose of a dam is to impound water for several reasons, like flood control, human water supply, irrigation, livestock water supply, energy generation and others. Embankment dams are common type of dams in use today. The two principal types of embankment dams are earth and rock-fill dams, depending on the predominant fill material used. Most dams are designed to fulfill their intended purposes and their construction and design depend on the volume of water they will retain.

Dam failures are usually caused by inadequate design, improper construction, or inadequate maintenance. Failure of the dam can cause considerable loss of capital investment, income, possible property damage, and loss of life. Loss of the reservoir can cause severe hardship for those dependent on it for their livelihood and can also upset the ecological balance of the area therefore, it requires a detailed investigation of the foundation for construction of safe and sustainable dam structure.

The major risk in the construction of any dam foundation is the uncertainty involved in predicting ground conditions and behaviors. Of course, the accuracy of these predictions will improve with increasing effort devoted to the subsurface investigation (Fang and John, 2006).

The successful design and construction of dams require a comprehensive site characterization and a detailed design of each feature. The design and construction of embankment dams is complex because of the nature of the varying foundation conditions and range of properties of the materials available for the use in the embankment. Therefore, the first step should be to conduct detailed geological and subsurface explorations, which characterize the foundation, abutments and potential burrow areas (U.S Army Corps of Engineers, 2004).

The stability of a structure depends up on the stability of the supporting earth materials. The important factors that require consideration are the location and depth of foundation. In deciding the location and depth, one has to consider the existence of active faults, failure surfaces, underground cavities, lateral transition of geological formations which are some of the most common subjects of concern for construction (Hailemariam Siyum, 2011).

Geophysical surveys have been applied to civil engineering investigations since the late 1920s, when seismic and resistivity surveys were used for dam site studies. Geophysical surveys are now used routinely as part of geological investigations to provide information on site parameters. All geophysical techniques are based on the detection of contrasts of different physical properties of materials like magnetic susceptibility, electrical resistivity, density and so on (U.S Department of the Interior, 2001).

Geophysical methods are extensively used in dam investigations, both on dam construction projects and in the assessment of the condition of existing dam structures. These methods help in identifying local areas of concern which have no surface expression. Moreover, the methods help to delineate boundaries between residual soils, weathered rocks and fresh rock. It is also possible to locate anomalous foundation features like dykes, cavities, fault zones and buried river channels (Fell et al., 2005).

Geophysical methods are used to determine the geological sequences and structures of subsurface rocks by the measurement of certain physical properties. Of these methods, the resistivity method is based on the fact that any subsurface variation in conductivity alters the pattern of current flow in the ground and therefore changes in the distribution of electric potential at the surface. Since the electrical resistivity of such factors as superficial deposits and bedrock differ from each other, the resistivity method may be used in their detection and to give their approximate thicknesses, relative positions and depths (Bell, 2007).

To investigate the ground structure and determine the individual formation resistivities, a series of measurements must be made with the electrodes in different positions. There are different techniques developed for different applications, like Vertical Electrical Sounding (VES):- a technique used to examine the vertical change in resistivity. The variation in resistivity with depth is interpreted quantitatively to provide resistivity and thicknesses of subsurface layers. Electrical Imaging is a recent development, which involves a combination of both traversing and sounding, to produce an image along a section through the subsurface. The magnetic method involves the measurement of variations in the total magnetic field of the earth, caused by local differences in the magnetization of the subsurface rocks and soils. A magnetic survey is rapid and easy to carry out. In the geological field, the magnetic method locates boundaries between rocks, which display magnetic contrasts, such as faults or dykes (McDowell et al., 2002).

Geophysical tools are routinely applied to a broad spectrum of geotechnical problems. Those tools are designed to measure specific parameters, and are generally used to measure spatial variation in these specific parameters within a study area, which are functions of the physical properties of the Earth's subsurface materials. Properly acquired and processed geophysical survey data are transformed into a physical property model. Which, finally it will be transformed to typical site model (Anderson et al., 2008).

1.2 Description of the Study Area

1.2.1 Location

The study area, Hizaeti Afras, is located near Wukro town, Tigray Regional State, North Ethiopia as shown in Figure 1.1. It is at about 820 km from the country's capital, Addis Ababa. The first 816km is accessible through an asphalted road that runs from Addis Ababa to Wukro and the remaining 4km is accessible through a dry weathered road. The study area is bounded by geographic UTM coordinates of 1524100m to 1524600m east and 562900m to 563450m north. The average elevation of the site is 1989m a.s.l and it falls under climatic zone of Weyna Dega.

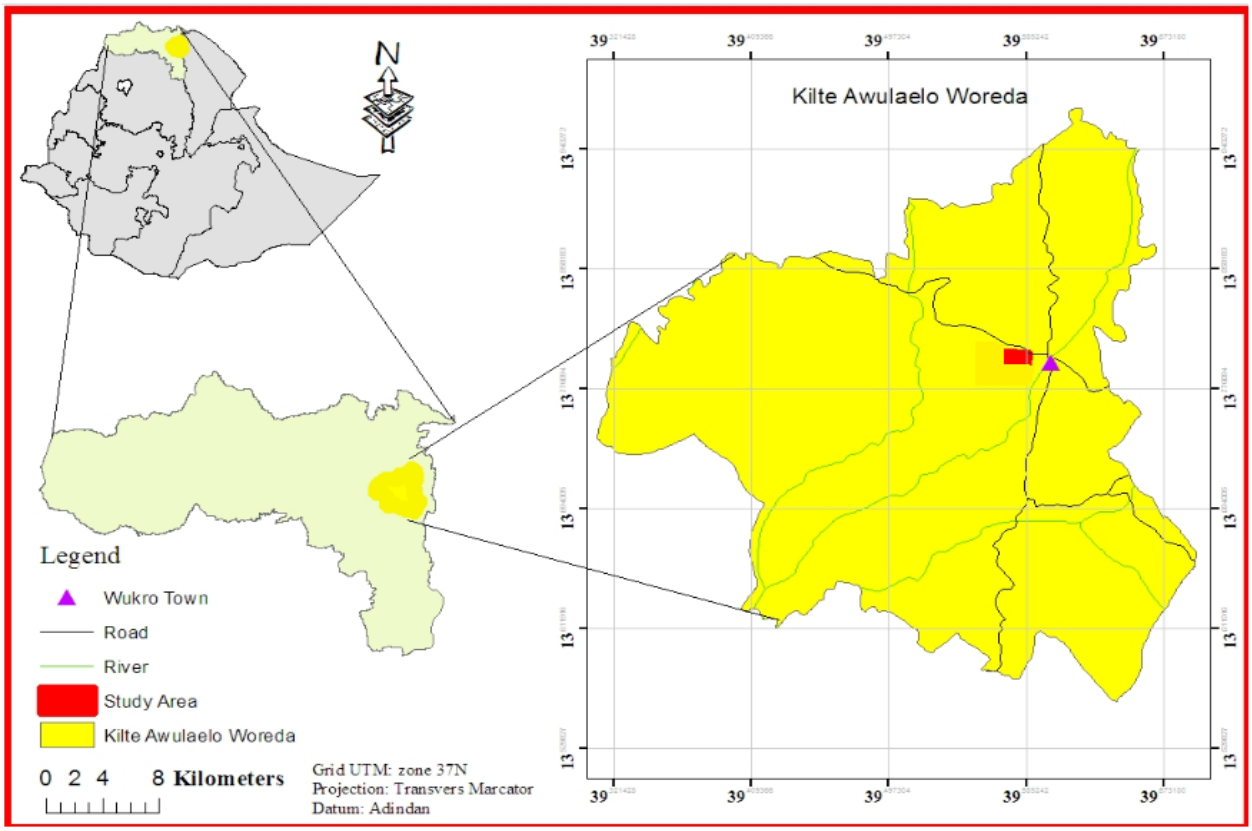

Figure 1.1 Location map of the study area.

1.2.2 Topography

The area, Hizaeti Afras, on which the dam is going to be constructed is a flat topography land bounded by a small hills on the western side, and a land with gentle slope on the eastern side, which will be used as the dam embankment. Figure 1.2 shows the general view of the dam the site with reservoir area in the foreground. The elevated ground (marked portion) on the far side is the face of the former dam body which is seen broken on the right hand side of the picture (north is towards the observer).

Figure 1.2 General view of Hizaeti Afras dam site.

1.3- Statement of the problem

Agriculture has been the backbone of Ethiopia's economy and it will be for the coming decades. However, the agricultural practices in the country, to the most part, are dependent on rain fall which makes it unsustainable because the rain fall depend on the year to year climatic conditions of the area. To make the agricultural economy more sustainable one way will be to support it with irrigation. For this purpose, the Tigray Regional State has constructed more than 50 micro dams in the last 20 years, out of which only few dams are functional at the time being.

About 70% of the total dams constructed have water retention problem. Out of these failed dams, 60% to 65% are related to geological and geo-technical reasons as indicated by various PhD/MSc researchers as well as by the preliminary assessment of the Tigray Water Resource, Mines and

Energy Bureau (Asmelash Abay, 2010). Although the magnitude of the problems differ from one project to another, the major technical problems observed in many of the micro dams include: excessive seepage, insufficient inflow, early sedimentation and structural and dam stability problems related to geology and geo-technical condition of the dam sites. At early stage of construction of the micro dams the region it was expected to irrigate about 2745ha in whole region. However, due to the failure of most dams, for reasons mentioned above, only 1000ha is currently under irrigation. Moreover, 34 million ETB used in constructing the failed dams has not fully been utilized to the intended target. The geological/geo-technical reasons for dam failure are associated with the predominantly alternating layers of fractured limestone beds with shale/marl, formations which are intensively affected by sills/dykes, solution cavities, shallow geological and geotechnical investigations and poor interpretation (Asmelash Abay, 2010).

Adigrat Diocesan Catholic Church Wukro Branch has planned to spend millions of Birr (around 15,399,444.5 Ethiopian Birr) for construction of a dam at the project site that is going to be used for irrigation purpose on the area specified above. The dam to be constructed is an Earth-fill dam type with crest length of 564m, dam crest width 5.0m and maximum height of 12m with embankment slopes of 2:1 on D/s and 2.5:1 on U/s sides. The size of the watershed area is 43.84km^2, which is sub-catchment of the Gereb-Giba watershed area that drains to Tekeze River. The hydrologic analysis of 18 years of rainfall data from Wukro station shows the mean annual rainfall to be 565mm and the calculated Peak Discharge from the catchment to be 142.52m^3/s. The storage capacity of the reservoir is 1.052Mm^3 including a dead storage volume of 0.274Mm^3. With proper usage the dam can irrigate 85ha annually. (TWMEB, 2011).

The available statistical data on dam failures suggests that earthen embankments experience the highest incidence of failure from all causes. Accordingly, the design and safety review of the Earth-fill embankments should be undertaken by dam engineers or geotechnical engineers experienced in this field. It is noted that dam failure initiated through conditions associated with dam foundation has been a commonly recorded feature (Dam Safety Committee, 2010). Consequently, the layout of the dam should avoid any sharp changes in the profile of the foundation, and the design should include assessment of foundation and foundation interface piping potential.

The sensitivity and safety of Earth dams is partly dependent on proper design which requires detailed foundation investigation to which geophysical investigations can contribute much.

However, the geotechnical study done so far by the Tigray Water Resource, Mines and Energy Bureau, for the proposed dam, did not include geophysical studies. Thus, to increase the sustainability of the dam project and its service life, and incorporate additional information in the dam design, detailed geophysical investigations are proposed to be deployed on the project site.

1.4- Objective

In addition to providing the required additional input that can be extracted from geophysical surveys to make the construction of the dam on sound basis, this project work has both general and specific objectives which are outlined as follows.

1. 4.1-General objective

The purpose of this study is to verify the suitability of the subsurface geological formations, ground conditions and structures for foundation of the proposed dam project based on results from geophysical investigations at the dam site.

1.4.2-Specific objectives

The project work has a number of specific objectives:

I. To map the subsurface geology and geological structures at the dam site.
II. To map subsurface resistivity stratification and to establish the geo-electric section of the dam site.
III. To determine the depth to the sound geological formation/bed rock.
IV. To correlate, wherever possible, the geotechnical results with findings from geophysical survey and come up with a detailed description of the subsurface that could be used as inputs to the dam design.
V. To get acquainted with the field practices, data processing techniques and interpretation schemes of geophysical methods when used in dam site investigation.

1.5- Methodologies and instrumentation

1.5.1 Methodologies

To achieve the objective of the research outlined above, secondary data was collected from respective offices, different literatures were reviewed and finally integrated geophysical methods were employed. The specific methods employed on the site included Electrical Resistivity Tomography (ERT), Electrical Resistivity Sounding (VES), and Magnetic Survey. Data were

collected along selected profiles and over random points (especially for magnetic method) well distributed to cover the investigation site. Electrical data that are collected using the above methods are analyzed using appropriate interpretation software like ProsysII, RES2DINV, Win RESIST, RESIX IP and Microsoft Excel. For the magnetic data, the analysis and plotting software used for this research are Oasis Montaj (version 6.4.2), Surfur (version 9) and Paint.

Accordingly maps and models are produced and interpreted to obtain information set out in the project objectives. The generalized flow chart of the methodological approach deployed for this investigation is described in Figure 1.3.

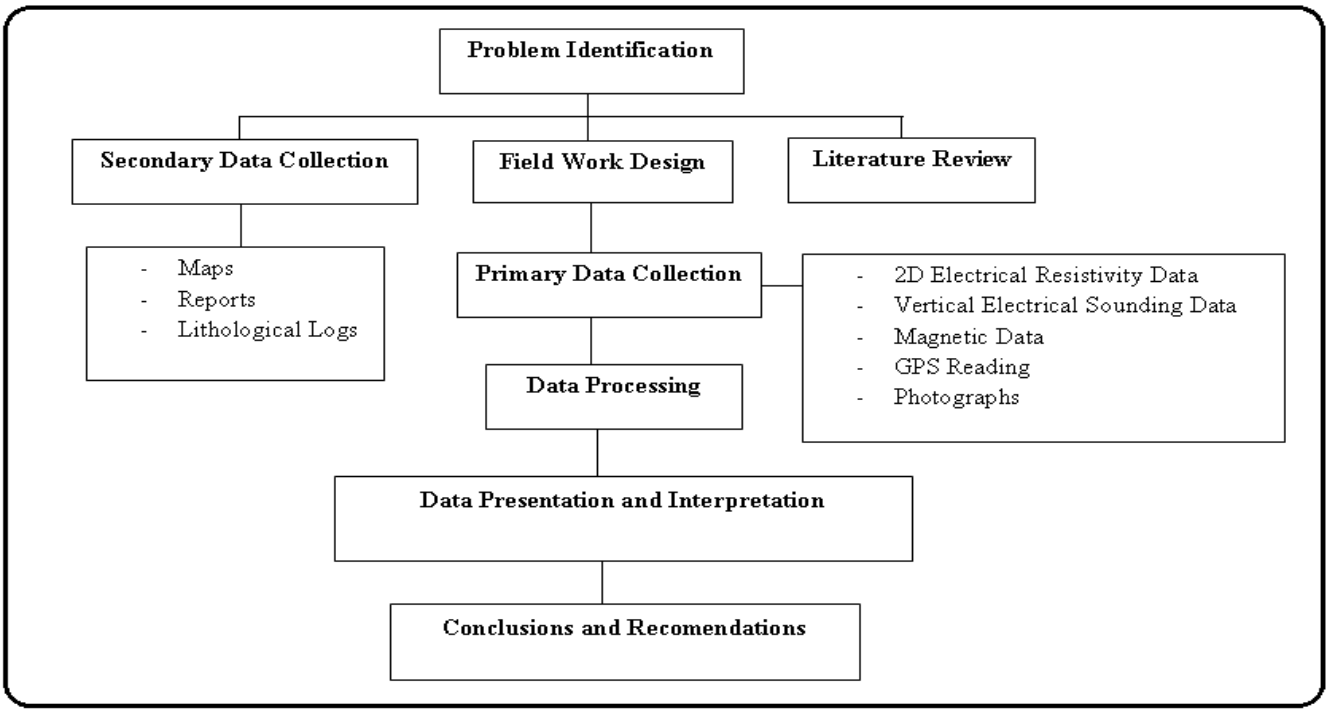

Figure 1.3 Flow chart of the methodologies applied for the investigation.

1.5.2 Instrumentation

The instruments which were used to collect the surface data include

1.5.2.1 The IRIS SYSCAL Resistivity and IP unit

The IRIS SYSCAL Pro R1 Plus Switch-72, used for the resistivity surveys, is a new all-in-one multimode resistivity imaging system featuring both multi electrode and resistivity measurements. It features an internal switching board for 72 electrodes and an internal 250 W power source. The output current is automatically adjusted to optimize the input voltage values and ensure the best

measurement quality. The system is designed to automatically perform pre-defined sets of resistivity measurements with roll-along capability. Four strings of cables with 18 electrodes each are connected together and to the resistivity meter. The strings were with standard electrode spacing of 5m. While working in multielectrode mode, the instrument is capable of conducting both vertical electrical sounding and profiling simultaneously. Its general specifications are

- Weather proof
- Shock resistant
- Operating temperature -20 to +70 ^{o}C
- Internal memory for 2700 readings
- Power supply; 2 internal rechargeable 12V

1.5.2.2 Proton Precession Magnetometer (Scintrex)

Proton precession magnetometer measures the resonance frequency of protons in the magnetic field to be measured, due to nuclear magnetic resonance. The instrument specifically used for this survey, the MP3 Scintrex made Proton Precession Magnetometer, can measure magnetic field with accuracy of 1nT. The resolving power reaches 0.1nT. Its general specifications are

- Measurement range 20,000nT to 100,000nT
- Measurement precision ± 1 nT
- Resolving power 0.1 nT
- Working temperature -10 to +50 ^{o}C

1.5.2.3 Global Positioning System (GPS)

Positions of the imaging lines, VES points and magnetic readings were made with Garmin model (eTrex Vista HC) hand held GPS using Adindan system.

1.6- Previous Work

In 2011 G.C the Tigray Water Resource, Mines and Energy Bureau has deployed a direct geotechnical method of investigation to collect information on the geotechnical properties of the geological formations within the specific site and to inspect construction material. According to their report, visual inspection of the site was carried out using traverses along river valleys and they have dug test pits of about 2m in selected positions and laboratory analysis of samples have been conducted. However, the laboratory results of the test pits were not interpreted for their

geotechnical significance in their report. Based on these investigations, it has been concluded and recommended as follows

- The foundation design should consider the pervious foundation condition as the dam site was also location of a smaller dam constructed earlier on the same site.
- To achieve effective cut-off trench a close follow up by the geologist is highly valuable.
- The buried river channel deposits have to be removed and filled with impervious material.
- The quantity of the proposed core material might be below the demand so further inspection is very important.

In addition to the above investigation, the Tigray Water Works Construction Enterprise has conducted vertical electrical sounding survey on the downstream side of the dam to investigate ground water for the Sheba Tannery S. Co in 2011. From the results of this survey three wells were drilled out of which one of them is dry. The well, which is used for lithological correlation with the resistivity stratification, is drilled at geographic location of 563432 E and 1524421 N.

1.7 Layout of the Thesis

The total work of this thesis is organized into six chapters. Chapter one of the thesis describes the introduction part which include general description of the study area, statement of the problem, objective, methodology and instrumentation and previous work. The second chapter incorporates geology, hydrogeology and seismicity of the study area. The topic which is covered in chapter three is theoretical background of the methods employed in the investigation. Chapter four covers the topics of data acquisition and processing. The interpretation of the different results is included in chapter five. The last chapter includes the conclusion and recommendation of the overall work of the thesis.

CHAPTER - 2

GEOLOGY, HYDROGEOLOGY AND SEISMICITY OF THE STUDY AREA

2.1 Geology

2.1.1 Regional Geology

The history of sedimentary basin in Tigray began in either the Ordovician or Carboniferous and probably ended in the lower Cretaceous before the eruption of the trap volcanic series (Beyth, 1972). During the Paleozoic, the channel-like basin was flooded followed by the deposition of Enticho sandstone and Edaga Arbi glacial on the basement rock. Transgression during the entire Triassic and most of Jurassic, sediments mostly Fluvial in origin, the socalled Adigrat sandstone was accumulated on the craton (Bosellini et at, 1997). Further, transgression of the sea deposited the Antalo limestone. The regression of the sea led to the deposition of the Agula Shale. A regional NW-SE uplift in the early Cretaceous is responsible for the forced withdrawal of the sea from the entire East Africa. This last regression of the sea deposited Amba Aradom formation, which is composed of siltstone, sandstone and conglomerate. Boselleni et al., (1997) suggested that the deposition of Amba Aradom formation is post tectonic in nature. Stratigraphy of the rock units constituting the region from oldest to youngest is Enticho sandstone and Edaga Arbi glacial, Adigrat sandstone, Antalo limestone, Agula shale, Amba Aradom formation and the Mekelle dolerite.

2.1.1.1 Enticho Sandstone and Edaga Arbi Glacials

These glacial rocks consists of two facies the tillite facies named Edaga Arbi Glacials and the Conglometate facies called the Enticho Sandstone. The Enticho sandtone is yellow to white, fine grained cemented by calcite, well bedded, finely cross bedded. It is unconformably overlying the folded basement rock. The Edaga Arbi glacial is gray to black in color with poorly sorted pebbles and boulders of granite at the base and gray silt, limestone inter bedded with thin silt beds at the top. The Edaga Arbi glacial uncomformably overlays the Enticho sandstone.

2.1.1.2 Adigrat Sandstone

The Adigrat Formation, which varies in thickness from a few meters to 800m, was originaly named

as Adigrat Sandstone after Adigrat town in Eastern Tigray by Blandford (1969) as cited in Beyth (1971). The sandstone is yellow to red color, fine to medium grained with variegated siltstone and clay. It is well rounded and well sorted mature sandstone with quartz grains comprising up to 90% of the rock. It shows a depositional basin trending NW-SE and could be Triassic to Callovian in age (Bosellini et al., 1997).

2.1.1.3 Antalo Limestone

The Antalo limestone is cliff forming rock, which is rich in fossils. It is conformably sandwiched between the lower Adigrat Sandstone and Lower Agula Shale. It contains well bedded crystalline limestone with shale and marl intercalations of various proportions. The Antalo limestone thins out at the Southern parts of the outlier with features that indicate a near shore environment; while in the northern part it thins probably due to the pre Ambaradon erosion (Beyth, 1971). Generally this limestone is non dolomitic intercalation of limestone and marl (Levitte, 1970) as cited in G/Medhin Berhane (2002).

2.1.1.4 Agula Shale

This unit is observed around Wukro town and Antalo Village. The Agula shale around Wukro is composed of very finely laminated black shale, marl and limestone containing gypsum. While the Agula shale around Antalo is silty clay in composition. The Agula shale comformably overlies on Antalo limestone while a clear angular unconformity separates it from the overlying Amba Aradom formation.

2.1.1.5 Amba Aradom Formation

This formation which is known as upper sandstone (Beyth, 1971) consists clay, silt, white to pink cross bedded sandstone and conglomerate accumulated in a fluvio lacustrine depositional environment.

2.1.1.6 Mekelle Dolerite

This unit occurs as sills, dykes and irregular bodies within the sedimentary successions. It is dark in color; fine to coarse grained and displays spheroidal weathering. It forms a sharp contact with

the Mesozoic sediments and the grain size becomes coarser at the mid of main sill body while it is fine grained at the contact zone.

2.1.2 Local Geology

The geology of the study area and its surrounding is dominated by quaternary alluvial deposits, Agula shale and limestone unit (Figure 2.1). The alluvial deposits are mainly composed of clay, silt, coarser sediments like sand gravel and boulders. The flat plain part of the reservoir that extends from the river centre towards the rim of the reservoir is dominated by river deposit material including clay, silt, sand and gravel. This layer has variable thickness that varies from 2m to 5m when seen in the river cut.

The Agula shale is an intercalation of shale, marl and limestone. This unit is found dominantly at the downstream and north east side of the study area. It is a variegated colour with an alternating grey, brown and pinkish. In most places the shale unit has friable nature and is lightly fractured. The light yellow coloured limestone unit is horizontally bedded, moderately to highly fractured. This unit is exposed mainly on the western bank of the dam axis and the reservoir.

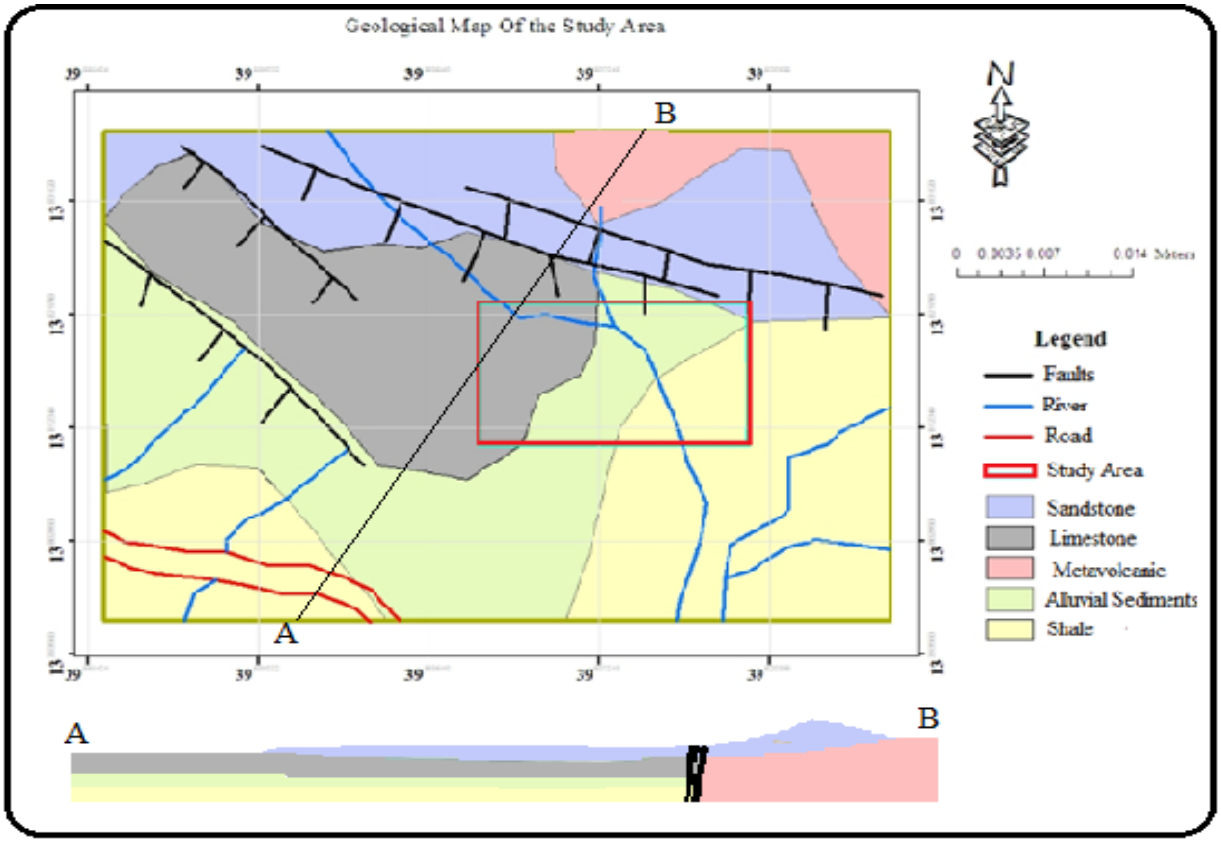

Figure 2.1 Geology map of the study area and its surrounding (T WMEB, 2011).

2.2 Hydrogeology of the Study Area

The prospect for groundwater at and around the study area is attributed to the interconnection of sedimentary grains, pattern of the fracture system and intensity of weathering. The depth of weathering depends mainly on the length of time for which the rock has been exposed to surface or near surface conditions and its original mineral composition.

The major lithologic units around the study area are the alluvial sediments and the Agula shale which comprises of an intercalation of shale, marl and limestone. The limestone and marl are moderately to highly fractured and jointed. From the hydrogeological point of view, the limestone, shale and marl units have secondary porosity associated with the weathering, fracturing and jointing nature of the units. While the alluvial deposits in the area have primary porosity mainly an inter-granular porosity is well observed. Accordingly the fractured limestone and the alluvial deposits are considered as good aquifers in the study area.

2.3 Seismicity of the Study Area

Seismic risk exists because of the convolution of three factors: seismic hazard, exposure to the hazard and vulnerability. The key to mitigating seismic risk therefore lies in controlling the vulnerability in the built environment by designing and building structures and facilities with sufficient resistance to withstand the effects of earthquakes. A seismic hazard assessment has to be performed to determine seismic loads to be considered in earthquake resistant design of structures (Bommer and Boore, 2004).

In seismically active region it may be possible to reduce loss of life and property damage by conducting detailed site specific prediction of seismic ground motion. With the knowledge of earthquake source mechanisms and path effects, detailed ground motion at any specific site of interest can be determined without waiting for earthquake to occur (Tilahun Mammo, 2005).

It is possible to simulate the ground motion and compute synthetic seismograms from theoretical considerations, which can then be used to model the response and improve the resistance of structures to damage from ground shaking. Based on the seismicity and the knowledge of the geology and tectonics the region can be broadly divided into three seismic source zones (Figure 2.2). These are the Afar Depression, the Escarpment and the Ethiopian Rift System. Each zone is, therefore distinguished by its own specific tectonic, geologic and seismic characteristics (Tilahun Mammo, 2005).

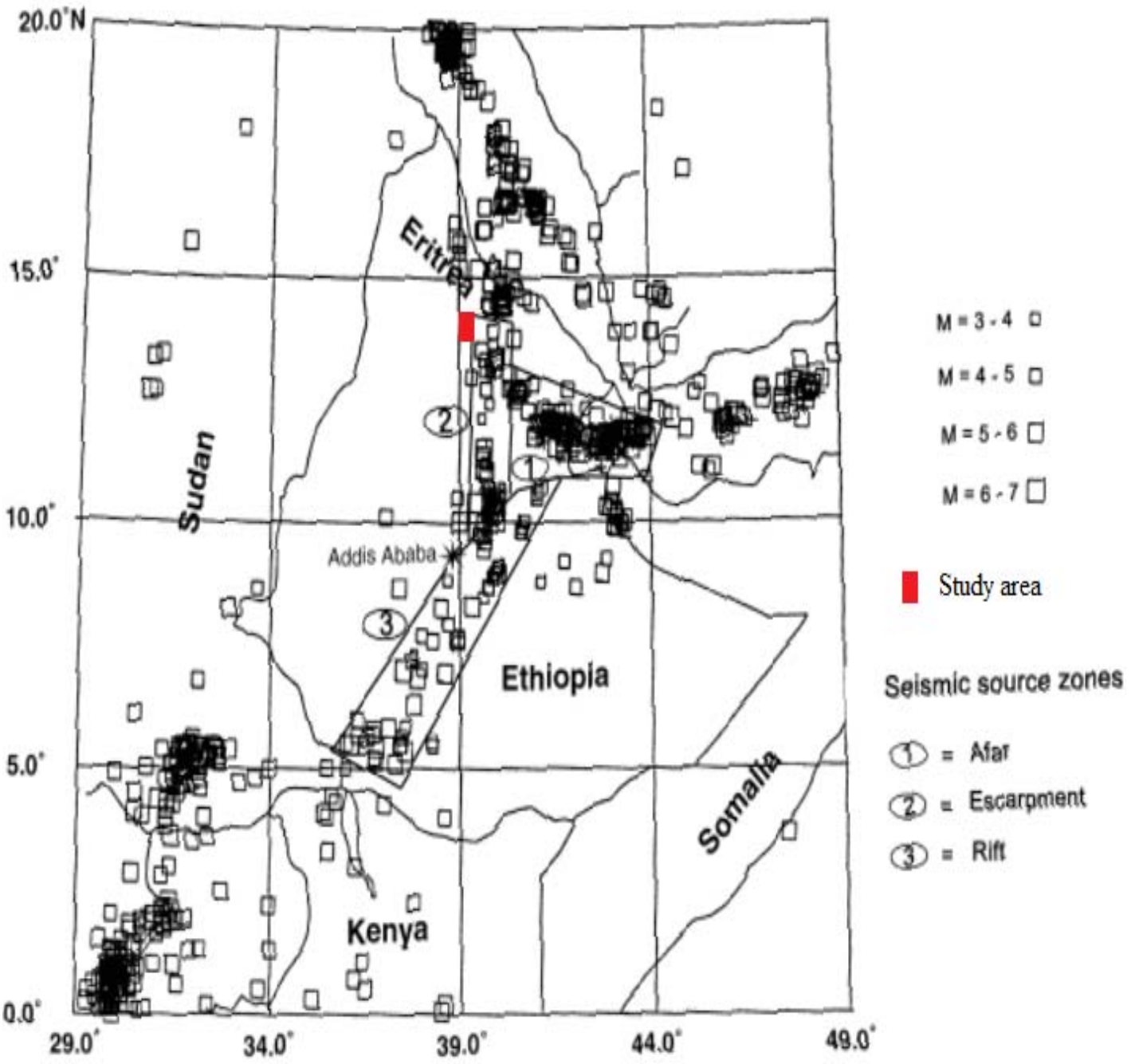

Figure 2.2 Seismicity of the Region with the Seismic Source Zones (Tilahun Mammo, 2005).

Earthquake activity in Eastern and Southern African region is characterized by the occurrence of destructive earthquakes which are controlled by the well known regional tectonic feature, the East Africa Rift System. Figure 2.3 shows the distribution of the earthquake epicenters in the region for the last periods (Midzi et al., 1999).

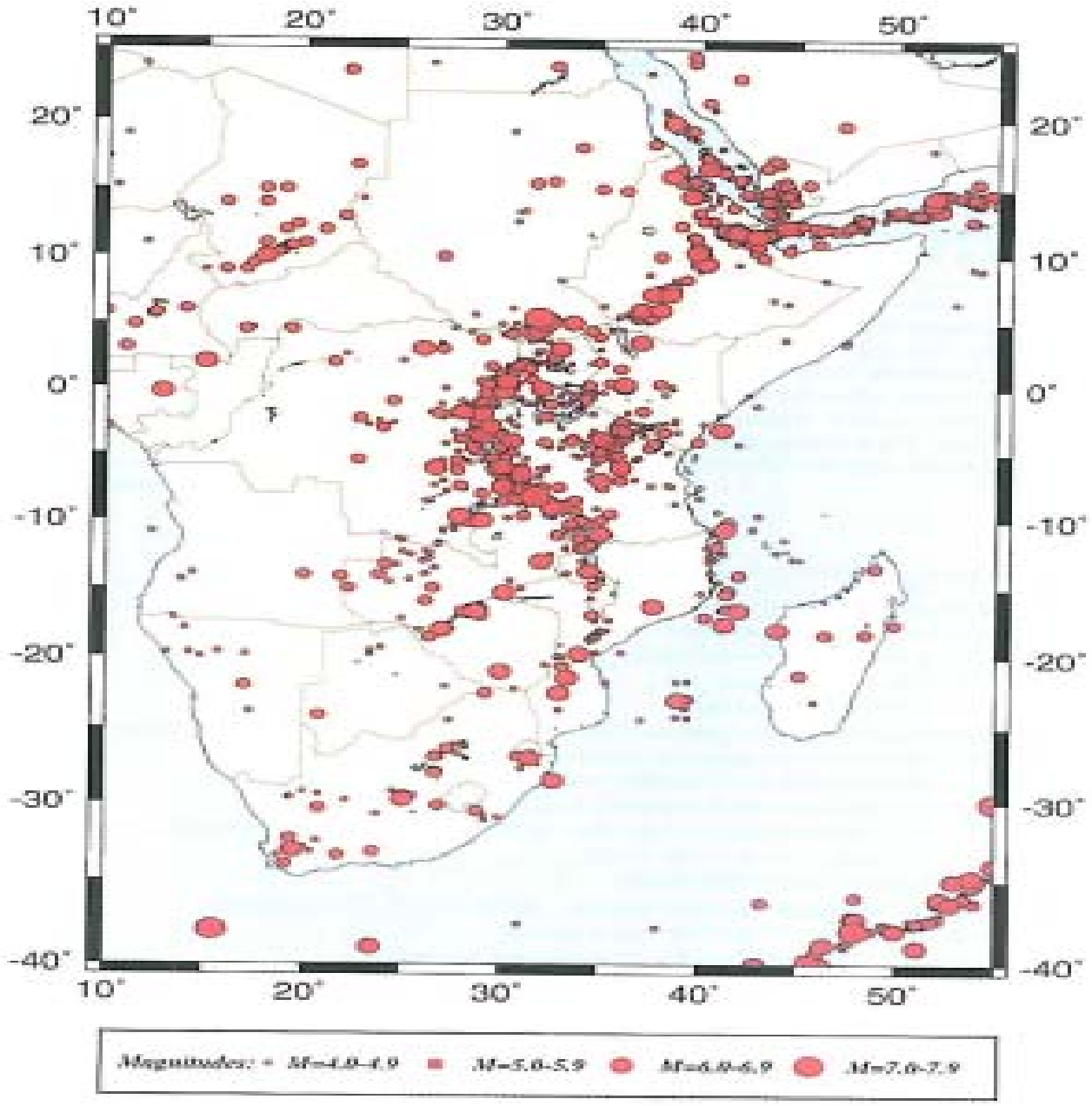

Figure 2.3 Seismicity of Eastern and Southern Africa. (Midzi et al., 1999).

The Ministry of Work and Urban Development of Ethiopia has established the Code of Standards for Seismic Loads in 1995. Accordingly, the country is divided into five zones depending on the known distribution of earthquakes (Figure 2.4) which are non damaging zone (0 zone), less damaging zone (zones 1 and 2) and zones of major damaging (zones 3 and 4). Moreover The ground acceleration ratio (α^o) depends on the seismic zones as given in Table 2.1 (Ethiopian Building Code Standard, 1995).

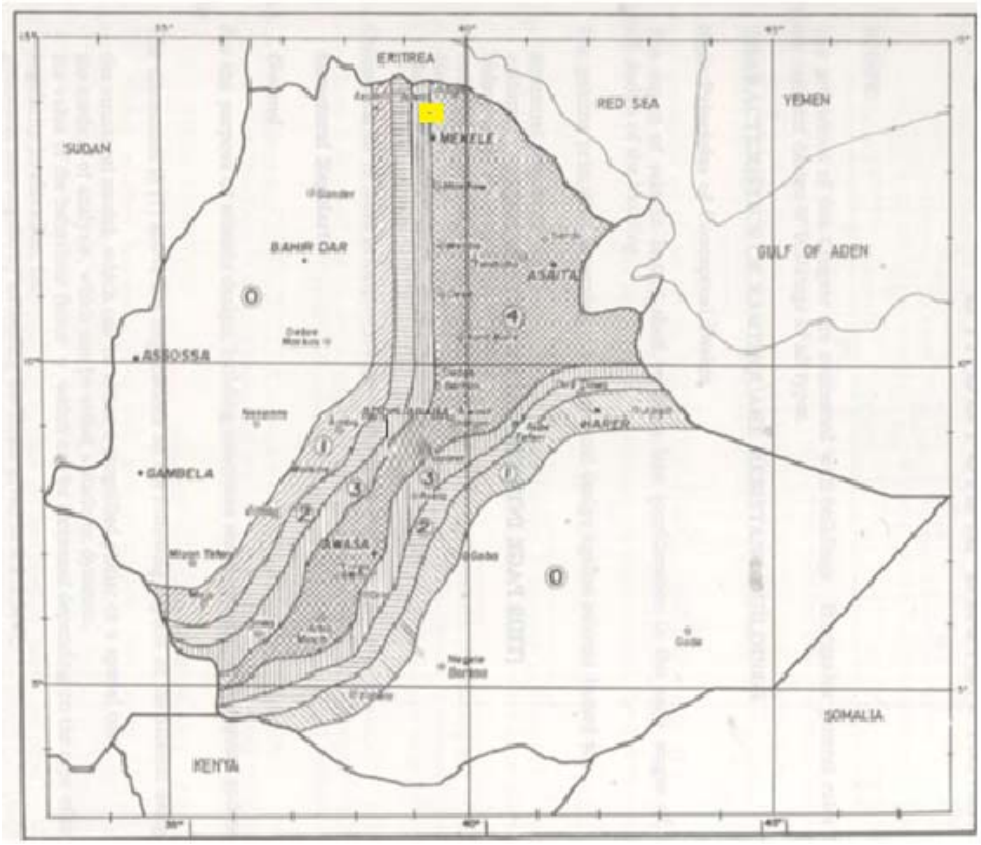

Figure 2.4 Seismic hazard map of Ethiopia (Ethiopian Building Code Standards, 1995) and location of the study area (shaded box)

Table 2.1 Ground acceleration ratio

Zone	4	3	2	1
α^{o}	0.1	0.07	0.05	0.003

According to Figures 2.2 and 2.3, the study site is very near to the Afar Escarpment seismic source zone and to the epicenter with higher magnitude (6.0 - 6.9). Moreover, based on the Ethiopian Building Code Standards zoning, the site falls at the boundary of zones 3 and 4, which are major damaging zones with ground acceleration of 0.07 to 0.10. This shows that the study area and its surrounding are so near to seismically active area. Therefore, considering the thick alluvial deposit, which is able to magnify the amplitude of earthquakes in the site and its vicinity to seismically active area of the Rift Escarpment the foundation design should incorporate all necessary conditions to withstand any seismic hazard.

CHAPTER - 3

THEORETICAL BACKGROUND OF THE METHODS OF INVESTIGATION

3.1 Direct Current Resistivity Method

3.1.1 Introduction

The resistivity method is used to study the subsurface in horizontal and vertical directions based on electrical resistivity variations resulted from difference in electrical properties. It is routinely used in engineering and hydrogeological investigations to investigate the shallow subsurface geology. In the resistivity method, artificially generated electric currents are introduced into the ground and the resulting potential differences are measured at the surface. Deviations from the pattern of potential differences expected from homogeneous ground provide information on the form and electrical properties of the subsurface inhomogeneities (Kearey et al., 2002).

The purpose of electrical resistivity surveys is to determine the subsurface resistivity distribution by making measurements on the ground surface. From these measurements, the true resistivity of the subsurface can be estimated. The ground resistivity is related to various geological parameters such as the mineral and fluid content, porosity and degree of water saturation in the rock. Electrical resistivity surveys have been used for many decades in hydrogeological, mining and geotechnical investigation (Loke, 1999).

The method has been used to locate fault zones, zones of deep weathering and cavities. It can also be used in the exploration of alluvial deposits where permeable gravel and sand beds can be distinguished from low permeability clays or rock. This capability has been applied in searches for construction materials beneath alluvial terraces and for foundation materials at dam site where significant alluvial deposits occur (McCann et al., 1987).

3.1.2 Fundamental Principles of resistivity

The fundamental physical law used in resistivity surveys is Ohm's Law that governs the flow of current in the ground (Telford et al., 1990). The equation for Ohm's Law in vector form for current flow in a continuous medium is given by

$$J = \sigma \mathrm{E}$$

(3.1)

where **σ** is the conductivity of the medium, **J** is the current density and **E** is the electric field intensity.

In practice, what is measured is the electric field potential. It is noted that in geophysical surveys the medium resistivity **ρ**, which is equals to the reciprocal of the conductivity (**ρ = 1/σ**), is more commonly used. The relationship between the electric potential and the field intensity is given by

$$\mathrm{E} = -\nabla \phi$$

(3.2)

Combining equation (3.1) and (3.2) we get

$$J = -\sigma \nabla \phi$$

(3.3)

In almost all surveys, the current sources are in the form of point source. In this case, over an elemental volume **ΔV** surrounding the current source **I**, located at (x_s, y_s, z_s) the relationship between the current density and the current is given by

$$\nabla J = \left(\frac{\mathrm{I}}{\Delta \nu} \right) \delta(x - x_s) \delta(y - y_s) \delta(z - z_s)$$

(3.4)

where **δ** is the Deric Delta function. Then equation 1.3 can rewritten as

$$-\nabla [\sigma(x, y, z) \nabla \phi(x, y, z)] = \left(\frac{\mathrm{I}}{\Delta \nu} \right) \delta(x - x_s) \delta(y - y_s) \delta(z - z_s)$$

(3.5)

This is the basic equation that gives the potential distribution in the ground due to a point current source. A number of techniques have been developed to solve this equation which is the forward modeling problem, i.e. to determine the potential that would be observed over a given subsurface structure. Considering a homogeneous subsurface and single point current source on the ground surface (Figure 3.1) the current flows radially away from the source, and the potential varies

inversely with the distance from the current source. The equipotential surface have a hemisphere shape, and the current flow is perpendicular to the equipotential surface.

The potential in this case is given by

$$\phi = \frac{\rho I}{2\pi r} \tag{3.6}$$

where '**r**' is the distance between the point in the medium (including the ground surface) and the electrode.

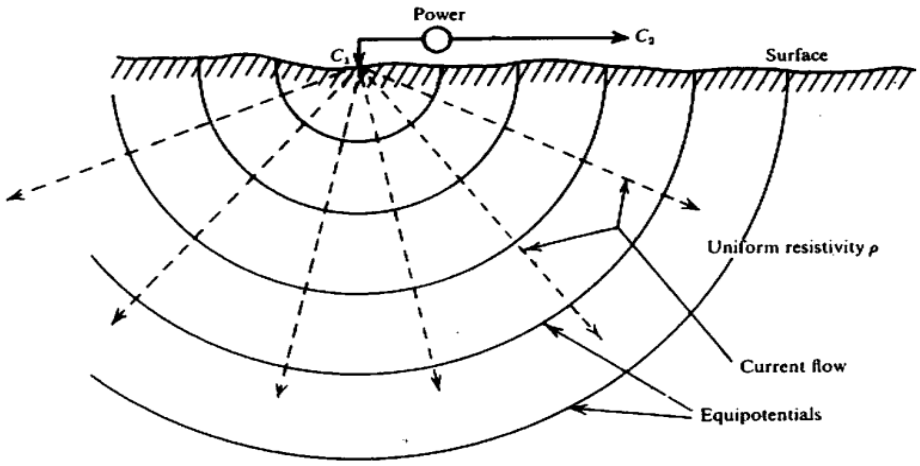

Figure 3.1 Point source of current at the surface of a homogeneous medium (Telford et al., 1990).

In practice, all resistivity surveys use at least two current electrodes, a positive current and a negative current source (Figure 3.2).

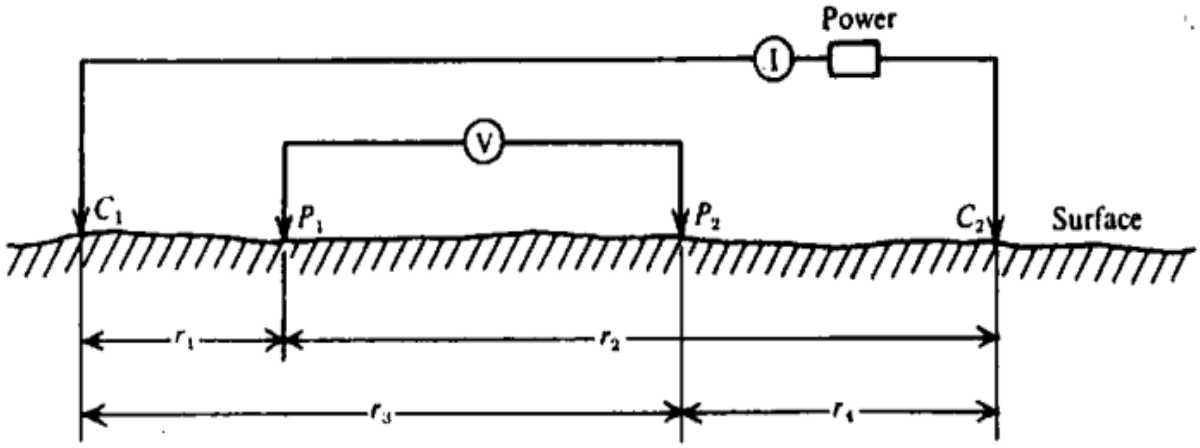

Figure 3.2 Two current and two potential electrodes on the surface (Telford et al., 1990)

The potential value in the medium from such a pair of electrodes is given by

$$\phi = \frac{\rho I}{2\pi}\left[\frac{1}{r_{c_1}} - \frac{1}{r_{c2}}\right]$$

(3.7)

where r_{c1} and r_{c2} are distances of the point from the first and second current electrodes.

In resistivity survey the measurement of potential difference between two points on the ground surface is done in an arrangement with 4 electrodes (Figure 3.2) and it is given by

$$\Delta\phi = \frac{\rho \mathrm{I}}{2\pi}\left[\frac{1}{r_{c_1 p_1}} - \frac{1}{r_{c_2 p_1}} - \frac{1}{r_{c_1 p_2}} + \frac{1}{r_{c_2 p_2}}\right]$$

(3.8)

The above equation gives the potential that would be measured over a homogenous half space with 4 electrodes array. However, actual field surveys are invariably conducted over an inhomogeneous medium where the subsurface resistivity has a 3-D distribution. The resistivity measurements are still made by injecting current into the ground through the two current electrodes C1 and C2 and measuring the resulting voltage difference at two potential electrodes (P1 and P2). From the current (**I**) and potential difference ($\boldsymbol{\Delta\phi}$) values, an apparent resistivity ($\boldsymbol{\rho_a}$) value is calculated.

$$\rho_{a = \mathrm{K}} \frac{\Delta\phi}{\mathrm{I}}$$

(3.9)

where K is a geometric factor that depends on the arrangement of the four electrodes and is given by

$$\mathrm{K} = \frac{2\pi r}{\left[\frac{1}{r_{c_1 p_1}} - \frac{1}{r_{c_2 p_1}} - \frac{1}{r_{c_1 p_2}} + \frac{1}{r_{c_2 p_2}}\right]}$$

The calculated resistivity value is not the true resistivity of the subsurface, but an apparent value that is the resistivity of a homogeneous ground that will give the same resistance value for the

same electrode arrangement. The objective of modern electrical resistivity surveys is to obtain true resistivity models for the subsurface which have a geological meaning. To determine the true subsurface resistivity from the apparent resistivity values is the inversion problem (Reynolds, 1997).

3.1.3 Electrode Arrays (Spreads)

Although many configurations of electrodes have been designed, only two are in common use. The Wenner configuration, in which the current and potential electrodes are maintained at an equal spacing '**a**' and the whole spread, is moved along a profile with the fixed value of '**a**'. In Schlumberger configuration the spacing is gradually increased about a fixed central point (Kearey et al., 2002).

3.1.3.1 Wenner Array

This is one of the most commonly used arrays in resistivity survey. It is very help full in determining lateral variations of the subsurface structures. In Wenner array the electrodes are uniformly spaced in a line. Setting $r_1 = r_4 = a$ and $r_2 = r_3 = 2a$ (Figure 3.3) and the apparent resistivity is given as

$$\rho_a = 2\pi a \frac{\Delta\phi}{I} \qquad (3.10)$$

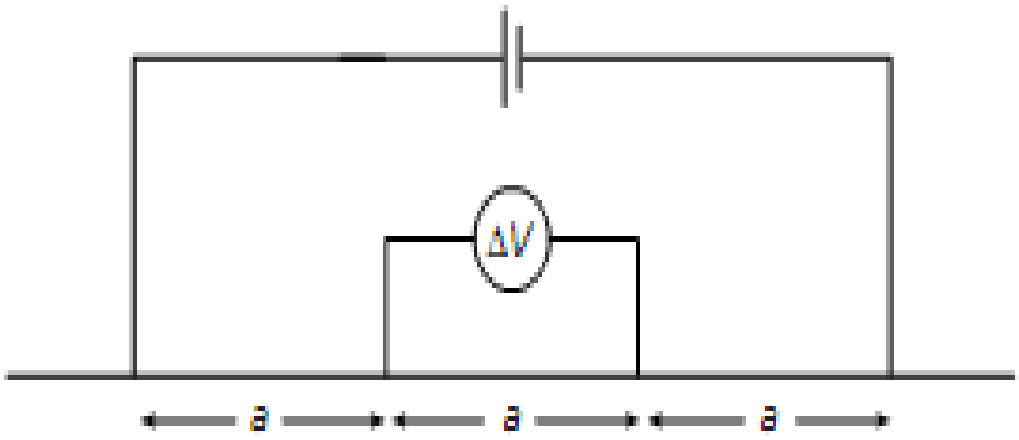

Figure 3.3 Wenner electrode configuration (Kearey et al., 2002).

3.1.3.2 Schlumberger Array

For the Schlumberger array the current electrodes are spaced much further apart than the potential electrodes (Figure 3.4). In this array all the electrodes move symmetrically from a measuring point. Schlumberger array allows determination of the resistivity variation of the subsurface geological setting as a function of depth and its apparent resistivity is given as

$$\rho_a = \frac{\pi L^2}{2l}\frac{\Delta\phi}{\mathrm{I}} \tag{3.11}$$

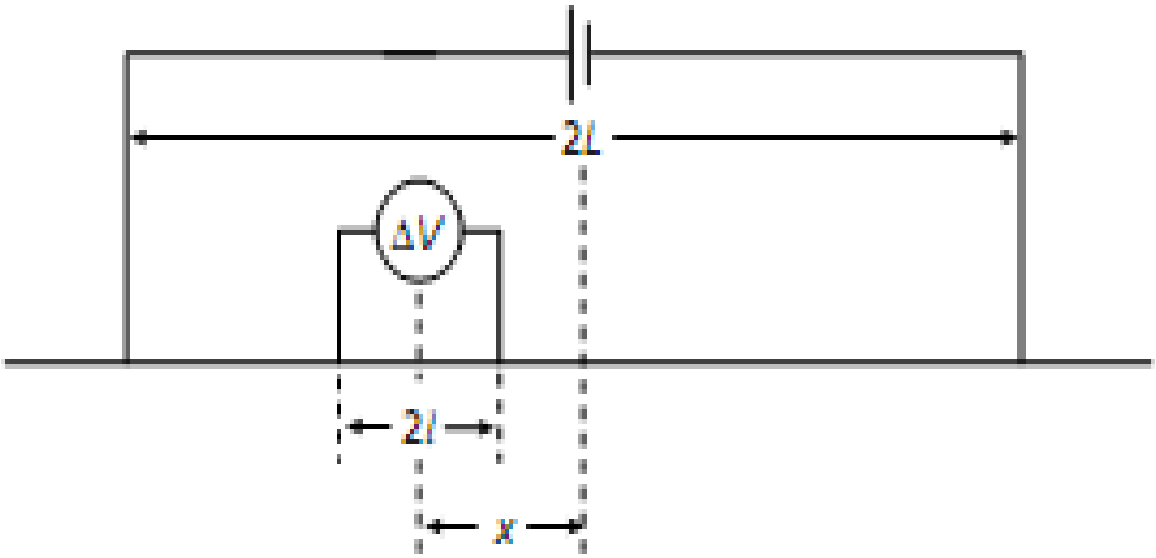

Figure 3.4 Schlumberger electrode configuration (Kearey et al., 2002).

3.1.4 Resistivity Field Procedures

Regardless of the specific electrode spread employed, there are really only two basic procedure in resistivity work. The particular procedure depends on whether one is interested in resistivity variations with depth or with lateral extent **(**Telford et al., 1990).

3.1.4.1 Vertical Electrical Sounding (VES) also known as electrical drilling. This is used mainly in the study of horizontal interfaces. The current and potential electrodes are maintained at the same relative spacing and the whole spread is progressively expanded about a fixed central point. Consequently, readings are taken as the current reaches progressively greater depths. The technique is extensively used in geotechnical surveys to determine overburden thickness (Kearey et al., 2002).

3.1.4.2 Constant Separation Traversing (CST), also known as electrical profiling. This method is used to determine lateral variations of resistivity. The current and potential electrodes are maintained at a fixed separation and progressively moved along a profile. This method is employed in mineral prospecting to locate faults or shear zones and to detect localized bodies of anomalous conductivity. It is also used in geotechnical surveys to determine variations in bedrock depth and the presence of steep discontinuities (Kearey et al., 2002).

3.1.5 Electrical Resistivity Tomography (ERT)

Electrical resistivity imaging is a technique in which many individual resistivity measurements are combined to produce a 2D or 3D resistivity cross-section of the subsurface. A linear array of electrodes is set into the ground and a computer system controls which two electrodes act as the current electrode. Measurements are acquired at various electrode separations and positions along the line to provide information at various lateral and vertical locations beneath the array.

The greatest limitation of the resistivity sounding method is that it does not take into account horizontal changes in the subsurface resistivity. A better approach to deal with the subsurface resistivity is a 2D model where the resistivity changes in the vertical and horizontal direction along the survey line are considered. In this case, it is assumed that resistivity does not change in the direction which is perpendicular to the survey line (Loke, 1999).

Electrical resistivity tomography is now a well established tool for environmental and engineering site investigation. ERT provides a relatively low cost and rapid means of generating spatial models of physical properties of the subsurface (Chambers et al., 2006).

3.1.5.1 Field Survey Method of 2D Electrical Imaging

One of the new developments in recent years is the use of 2D electrical imaging surveys to map areas with moderately complex geology. Such surveys are usually carried out using a large number of electrodes, 25 or more, connected to a multi core cable (Figure 3.5). The multi core cable is attached to an electronic switching unit which is connected to a laptop computer. The sequence of measurements to take, the type of array to use and other survey parameters is normally entered into a text file which can be read by a computer program in a laptop computer. In typical survey, most of the fieldwork is in laying out the cable and electrodes. After that, the measurements are taken automatically and stored in the computer (Griffiths and Barker, 1993).

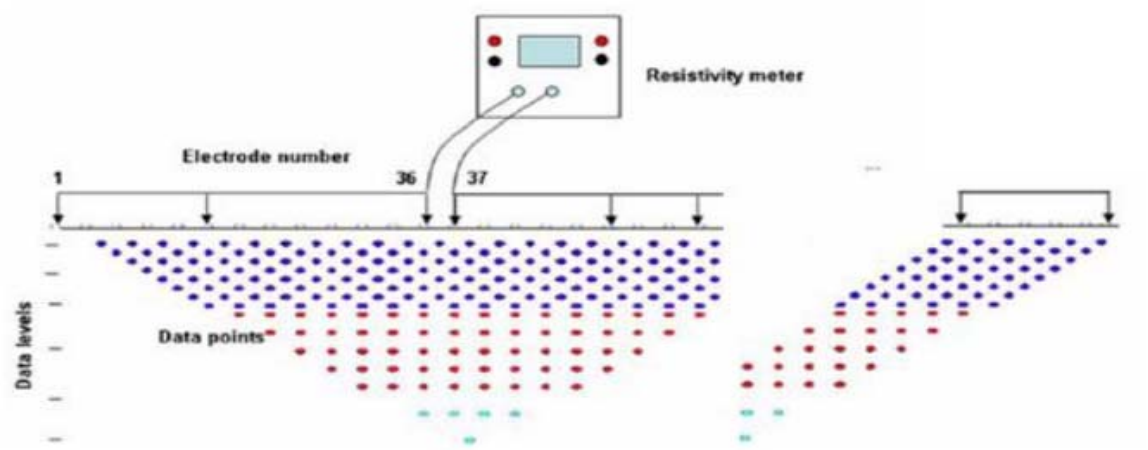

Figure 3.5 Generalized survey procedures with the main sequence in the left, roll-along in the right and data points of 2-D resistivity imaging (Tigstu Haile, 2010)

3.1.5.2 Forward Modeling

Forward modeling is a technique to model a subsurface by estimating the actual resistivity of the different geological structures. The estimation is made by calculating the apparent resistivity of the respective ground structure using the fundamental theoretical electrical equations.

The resistivity response for a 2-D model is calculated and displayed as a pseudo-section for comparison with the original field data. This approach is used to generate realistic subsurface geometries in definable model structures (Reynolds, 1997). Forward modeling operates through a process which divides the subsurface is into a large number of small rectangular cells (McDowell et al., 2002).

3.1.5.3 Basic Inverse Theory

Geophysical inversion is a method which finds a model that gives a response that is similar to the actual measured values. The model is an idealized mathematical representation of a section of the earth. The model has a set of model parameters of physical quantities which are required to be estimated from the observed data. The model response is the synthetic data that can be calculated from the mathematical relationships defining the model for a given set of model parameters. All inversion methods essentially try to determine a model for the subsurface whose response agrees with the measured data subject to certain restrictions.

In all optimization methods, an initial model is modified in an iterative manner so that the difference between the model response and the observed data values is reduced. The set of observed data can be written as a column vector **y** given by

$$y = col(y_1, y_2, ...y_m) \tag{3.12}$$

where **m** is the number of measurements. The model response **f** can be written in a similar form

$$f = col(f_1, f_2, ... f_m) \tag{3.13}$$

The difference between the observed data and the model response is given by discrepancy vector **g** that is defined by

$$g = y - f \tag{3.14}$$

In the least square optimization method, the initial model is modified such that the sum of squares error **e** of the difference between the model response and the observed data values is minimized and is given as (Loke, 1999).

$$e = \sum_{i=1}^{n} g^2 = g^T g \tag{3.15}$$

The above equation can be rewritten as

$$e = \sum_{i=1}^{n} \sqrt{(m_i - r_i)^2} \tag{3.16}$$

where, r_i is the i^{th} calculated reisitivity value, m_i is the i^{th} observed apparent resistivity and n is number of measured data. To get minimum **e** (root mean square error, RMS) the smoothness constrained least square method (deGroot-Hedlin and Constable, 1990) is used. It is given as

$$d(J^T J + U.F) = J^T g - UFr \tag{3.17}$$

where, $F = f_x f_x^T + f_z f_z^T$, f_x is vertical flatness filter, J is matrix of partial derivatives, U is damping factor, d is model perturbation factor, r is a vector containing the logarithm of the model resistivity value and g is discrepancy vector.

3.1.6 The relationship between geology and resistivity

Resistivity surveys give a picture of the subsurface resistivity distribution. To convert the resistivity picture to a geological picture, some knowledge of typical resistivity values for different types of subsurface materials and the geology of the area surveyed is important. Igneous and

metamorphic rocks have high resistivity values, which greatly depend on degree of fracturing and the percentage of the fractures filled with water. Sedimentary rocks have lower resistivity value because is usually porous and have higher water content (Loke, 1999). Resistivity of some common rocks is given in Table 3.1 (Loke, 1999).

Table 3.1 Resistivity of some common rocks

Material	Resistivity (Ω.m)	Conductivity (Siemen/m)
Igneous and Metamorphic Rocks		
Granit	5×10^{3} - 10^{6}	$10^{-6} - 2 \times 10^{-4}$
Basalt	$10^{3} - 10^{6}$	10^{-6} -10^{-3}
Slate	$610^{2} - 4 \times 10^{7}$	$2.5 \times 10^{-8} - 1.7 \times 10^{-3}$
Marble	$10^{2} - 2.5 \times 10^{8}$	$4 \times 10^{-9} - 10^{-2}$
Quartzite	10^{2} - 2×10^{8}	$5 \times 10^{-9} - 10^{-2}$
Sedimentary Rocks		
Sandstone	8 -4×10^{3}	$2.5 \times 10^{-4} - 0.125$
Shale	20 -2×10^{3}	$5 \times 10^{-4} - 0.05$
Limestone	50 - 4×10^{2}	$2.5 \times 10^{-3} - 0.02$

3.2 The Magnetic Method

3.2.1 Introduction

Magnetic method is a versatile, low cost, easy to operate geophysical tool applicable to quite different subsurface exploration problems (Kirsch, 2009). It can be used in a wide variety of applications such as locating pipes and cables in the very near surface, engineering site investigations and regional geological mapping to determine gross structure (Reynolds, 1997).

3.2.2 Basic Concepts

The Earth's large scale magnetic field is superimposed by small scale magnetic anomalies related with magnetized rocks. Magnetization is the parameter corresponding to density in the gravity method. Magnetization is a vector quantity which is related with the concept of north and South Pole of a magnet (Kirsch, 2009).

Within the vicinity of a bar magnet a magnetic flux is developed which flows from one end of the magnet to the other (Figure 3.6). This flux can be mapped from the directions assumed by a small compass needle suspended within it. The points within the magnet where the flux converges are known as the poles of the magnet. A freely suspended bar magnet similarly aligns in the flux of the Earth's magnetic field. The pole of the magnet which tends to point in the direction of the Earth's north pole is called positive pole, and this is balanced by the south seeking or negative pole (Kearey et al., 2002).

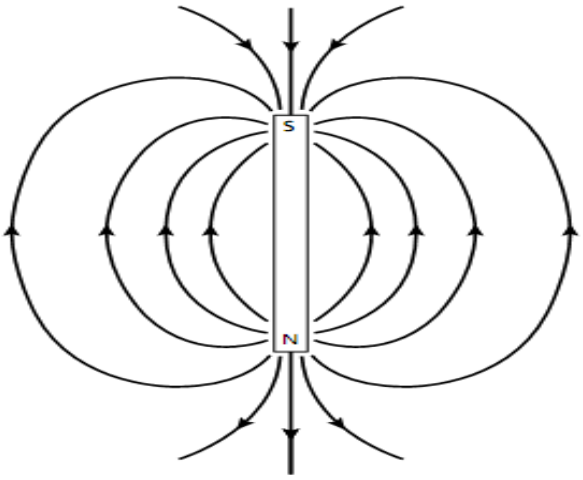

Figure 3.6 Magnetic flux surrounding a bar magnet (Kearey et al., 2002).

The force of **F** between two magnetic poles of strengths m_1 and m_2 separated by a distance r is given by

$$F = \frac{\mu_o m_1 m_2}{4\pi\mu_R r^2} \tag{3.18}$$

where μ_0 and μ_R are constants corresponding to the magnetic permeability of vacuum and the relative magnetic permeability of the medium separating the poles. The force is attractive if the poles are of different sign and repulsive if they are of like sign.

The magnetic field **B** due to a pole of strength m at a distance r from the pole is defined as the force exerted on unit positive pole at that point

$$B = \frac{\mu_o m}{4\pi\mu_R r^2} \tag{3.19}$$

Magnetic fields can be defined in terms of magnetic potentials. For a single pole of strength m, the potential **V** at a distance r from the pole is given by

$$V = \frac{\mu_o m}{4\pi\mu_R r} \tag{3.20}$$

The magnetic field component in any direction is then given by the partial derivative of the potential in that direction.

In the SI system of units, magnetic parameters are defined in terms of the flow of electric current. If a current is passed through a coil consisting of several turns of wire, magnetic flux flows through and around the coil annulus which arises from a magnetizing force **H.** The magnitude of **H is** proportional to the number of turns in the coil and the strength of the current, and inversely proportional to the length of the wire, so that **H** is expressed in Am^{-1}. The density of the magnetic flux, measured over an area perpendicular to the direction of flow, is known as the magnetic induction of magnetic field **B** of the coil. **B** is proportional to **H** and the constant of proportionality μ is known as the magnetic permeability (Reilly, 1972).

Common magnets exhibit a pair of poles and are therefore referred to as dipoles. The magnetic moment **M** of a dipole with poles of strength m a distance l apart is given by

$$M = ml \tag{3.21}$$

The magnetic moment of a current carrying coil is proportional to the number of turns in the coil, its cross-sectional area and the magnitude of the current.

When a material is placed in a magnetic field it may acquire a magnetization. This phenomenon is referred to as induced magnetization. The intensity of induced magnetization **J** of a material is defined as the dipole moment per unit volume of the material

$$J = \frac{M}{LA} \tag{3.22}$$

In other way the induced intensity of magnetization is proportional to the strength of the magnetizing force **H** of the inducing field.

$$J = \kappa H \tag{3.23}$$

where **K** is the magnetic susceptibility of the material.

In a vacuum the magnetic field strength **B** and magnetizing force **H** are related by

$$B = \mu_o H \tag{3.24}$$

where, μ_0 is the permeability of vacuum (4π x 10^{-7}Hm^{-1}). Air and water have similar permeability to μ_0 and so this relationship can be taken to represent the Earth's magnetic field when it is undisturbed by magnetic materials. When a magnetic material is placed in this field, the resulting magnetization gives rise to an additional magnetic field in the region occupied by the material, whose strength is given by $\mu_0 J$. Within the body the total magnetic field or magnetic induction, **B** is given by

$$B = \mu_o H + \mu_o J \tag{3.25}$$

Substituting equation (3.23)

$$B = \mu_o H + \mu_o \kappa H = (1 + \kappa)\mu_o H = \mu_R \mu_o H$$

The magnetic permeability **μ**is thus equal to the product of the relative permeability and the permeability of vacuum, and has the same dimensions asμ_0**.** For air and water μ_R is close to unity.

3.2.3 The Earth's Magnetic field

The geomagnetic field at or near the surface of the Earth originates largely from within and around the Earth's core. Current induced in the Earth by external field and induced magnetization of crustal rocks; also contribute to the overall geomagnetic field. The geomagnetic field is produced by electric currents induced within the conductive liquid outer core as a result of slow convective movements within it (Figure 3.7). It is for this reason that the analogy of the Earth's field to that induced by an electromagnet is preferred to that of a permanent magnetized bar (Reynolds, 1997).

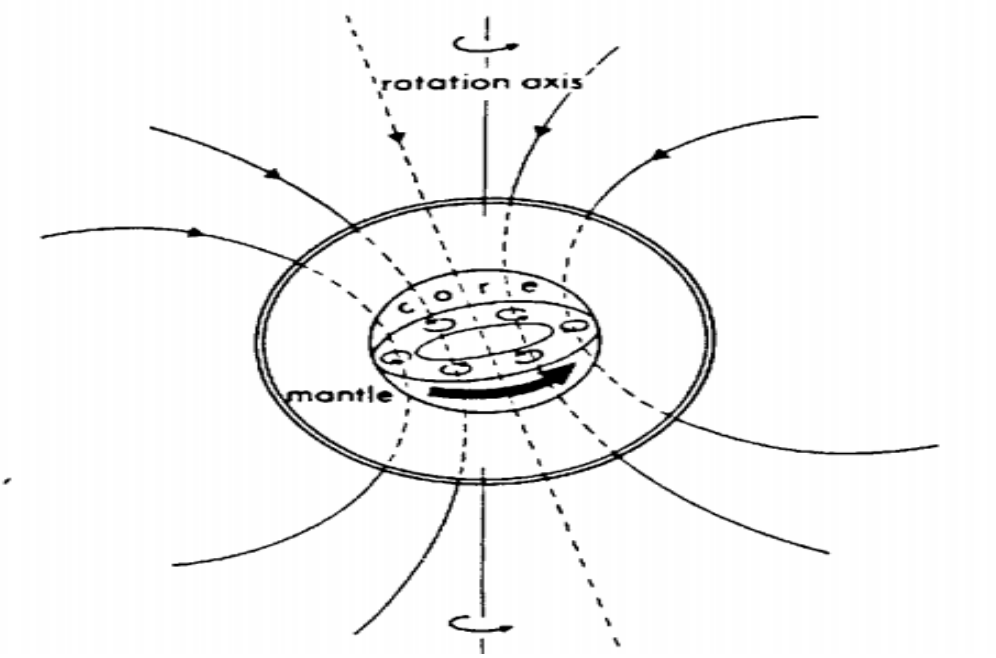

Figure 3.7 Schematic of the cause of the majority of the Earth's magnetic field (Sharma, 1986)

3.2.4 Magnetic Survey and field procedure

The aim of magnetic survey is to investigate subsurface geology on the basis of anomalies in the Earth's magnetic field resulting from the magnetic properties of the underling rocks. A survey can be performed on land, at sea and in the air. Consequently, the technique is widely employed and the speed of operation makes the method very attractive (Kearey et al., 2002).

Magnetic measurements are performed in grids or on profiles. Repeated magnetometer readings at base station have to be performed to record periodic and non periodic magnetic fluctuations related with ionospheric processes (Kirsch, 2009).

The method involves the measurement of variations in the total magnetic field of the earth, caused by local differences in the magnetization of the subsurface rocks and soils. The greatest application in engineering studies is it locates boundaries between rocks, which display magnetic contrasts, such as faults or dykes. Significant progress has been made in the mathematical modeling of magnetic data, particularly of the variations in 1-D visualization. It is also possible to produce 2-D geological models from the magnetic data (McDowell et al., 2002).

In ground based surveys, it is important to establish a local base station in an area away from suspected magnetic targets or magnetic noise and where the locale field gradient is relatively flat. A base station should be quick and easy to relocate and reoccupy. The precise approach to the

survey will depend on the type of equipments. If a manual push button proton magnetometer is deployed, the exact time of occupation of each station is needed and at least three reading of the total field strength should be recorded. Each of the three values should be within ± 1or 2 nT and then an average of these three readings is calculated. As the survey progresses, the base station must be reoccupied every half an hour in order to compile a diurnal variation curve for later correction. Next to data entry, where required, there should be any comments about the terrain or other factors that may be considered to be important or relevant to subsequent data processing and interpretation (Reynolds, 1997).

3.2.5 Field Equipments

Magnetic field measurements are carried out with magnetometers. Earlier purely mechanical magnetometers have completely been replaced by electronic instruments based on various physical processes. The most common magnetometers currently in use are proton precession magnetometers composed of a portable sensor and an electronic unit for display and storage of the data. Proton precession magnetometers measure the total intensity of the Earth's magnetic field vector at a resolution of 0.1–1 nT (Kirsch, 2009).

3.2.6 Reduction of Magnetic Observation

The Earth's magnetic field changes over a daily period and these are what are called the diurnal variations. These are caused by changes in the strength and direction of currents in the ionosphere. On a magnetically quiet day, the changes are on average around 50 nT but with maximum amplitudes up to 200 nT at the geomagnetic equator (Reynolds, 1997).

Therefore, one effect that must be compensated in magnetic survey is the variation in intensity of the geomagnetic field at the Earth's surface during the course of a day which is diurnal variation. It can be corrected by installing a constantly recording magnetometer at a fixed base station within the survey area by visiting a base station periodically (Lowrie, 2007).

The geomagnetic correction is a technique that removes the effect of geomagnetic references field from the survey data. The most rigorous method of geomagnetic correction is the use of the International Geomagnetic Reference Field (IGRF) (Kearey et al., 2002). For small sized area of investigation only diurnal corrections could be applied (Kirsch, 2009).

The total field anomaly (**ΔB**) is calculated based on the following formula from the observed magnetic data ($\mathbf{B_{obs}}$), the diurnal variation (**δB**) which, will be generated from the base station

measurement and the dipole field ($\mathbf{B_d}$) which will be determined from the international geomagnetic reference field.

$$\Delta B = B_{obs} \pm \delta B - B_d \tag{3.26}$$

3.2.7 Analytical Signal

Due to the dipolar nature of the geomagnetic field, magnetic anomalies observed anywhere other than the poles are asymmetric even when the causative body distribution is symmetric. This property complicates the interpretation of magnetic data. Reduction to the pole (RTP) is a technique that converts magnetic anomaly to symmetrical pattern which would have been observed with vertical magnetization. Analytical signal is a suitable quantity that can be calculated in frequency domain and its magnitude is independent of the magnetization direction thus; it can be used as RTP operator. Analytical signal is formed through the combination of the horizontal and vertical gradient of the magnetic anomaly. The analytical signal has a form over causative body that depends on the location of the body (horizontal coordinates and depth) but not on its magnetization direction (Roest et al., 1992).

In the reduction to the pole procedure, the measured total field anomaly is transformed into the vertical component of the field caused by the same source distribution magnetized in the vertical direction. The acquired anomaly is therefore the one that would be measured at the north magnetic pole, where induced magnetization and ambient field both are directed downwards (Blakely, 1995).

The amplitude function of the analytical signal is defined as the square root of the squared sum of the vertical and two horizontal derivatives of the magnetic field anomaly

$$|A(x,y)| = \sqrt{\left(\frac{\partial M}{\partial x}\right)^2 + \left(\frac{\partial M}{\partial y}\right)^2 + \left(\frac{\partial M}{\partial z}\right)^2}$$

where |A(x,y)| and M are the amplitudes of the analytic signal and the magnetic anomaly field intensity respectively. This signal exhibits maxima over magnetization contrasts, independent of the ambient magnetic field and source magnetization directions (Salem et al., 2002).

3.2.8 The Tilt Angle Derivative

One important goal in the interpretation of magnetic data is to determine the magnetic source parameter such as location of boundary and depth based on the use of derivatives of magnetic field.

Tilt angle is defined as

$$\theta = \tan^{-1}\left[\frac{\partial M}{\partial z} \Big/ \frac{\partial M}{\partial h}\right]$$

where $\frac{\partial M}{\partial h} = \sqrt{\left(\frac{\partial M}{\partial x}\right)^2 + \left(\frac{\partial M}{\partial y}\right)^2}$

and $\frac{\partial M}{\partial x}$, $\frac{\partial M}{\partial y}$, $\frac{\partial M}{\partial z}$ are first order derivatives of the magnetic field (M) in the direction of x, y and z.

Since tilt angle is an inverse trigonometric function all resultant values are between -90^o and +90^o this fact makes this relationship function like an automatic gain control, therefore it normalizes all amplitudes to this range. The tilt derivatives vary markedly with inclination but for inclinations of 0^o to 90^o its zero crossing is located close to the edges of the model structure (Miller and Singh, 1994).

3.2.9 Magnetic Properties of Rocks and minerals

Magnetism of rocks is related with the magnetism of the rock forming minerals. Diamagnetic minerals like quartz and calcite have negative susceptibilities of the order of 10-5. Minerals like feldspars and micas are paramagnetic and have higher (positive) susceptibilities (10-4 – 10-2). The positive susceptibility of ferromagnetic minerals like magnetite (k ~ 1 - 10) is even larger by some orders of magnitude and in general most important for the magnetization of rocks (Kirsch, 2009).

Magnetic susceptibility is an extremely important property of rocks and to magnetic exploration method. The whole rock susceptibility can vary considerably owing to a number of factors in addition to mineralogical composition such as alignment and shape of the magnetic grains dispersed throughout the rock (Reynolds, 1997).

However the susceptibility of a rock mainly depends on its magnetite content. Sediments and acidic igneous rocks have small susceptibilities whereas basalts, dolerites, gabbros and serpentinites are usually strongly magnetic. Weathering generally reduces susceptibility because magnetite is oxidized to hematite. The susceptibilities, in rationalized SI units, of some common rocks and minerals are given in Table 3.2 (Milson, 2003).

Table 3.2 Magnetic susceptibilities of Limestone (Milson, 2003)

No	**Rocks and Minerals**	**K**
9	Limestone	0.00001 – 0.0001

CHAPTER - 4

DATA ACQUISTITING AND PROCESSING

4.1 Data Acquisition

4.1.1 2D Electrical Resistivity Data

The 2D imaging data were collected using IRIS SYSCAL Pro R1 Plus Switch 72 instrument. The instrument consist 72 electrodes which are connected to the reel cable at every 5m spacing using connectors. This instrument runs both vertical electrical sounding and profiling simultaneously and it calculates the apparent resistivity of a point from the current, potential difference and electrode spacing at any four electrodes of the array. The 2D Electrical Imaging data are acquired systematically along traverses which were selected to collect a representative and detailed information about the area around the dam foundation.

Totally four profile lines were selected for the survey, in which three of the profiles are nearly parallel to the dam axis with E-W orientation while one profile is perpendicular to the dam axis with N-S orientation (Figure 4.1).

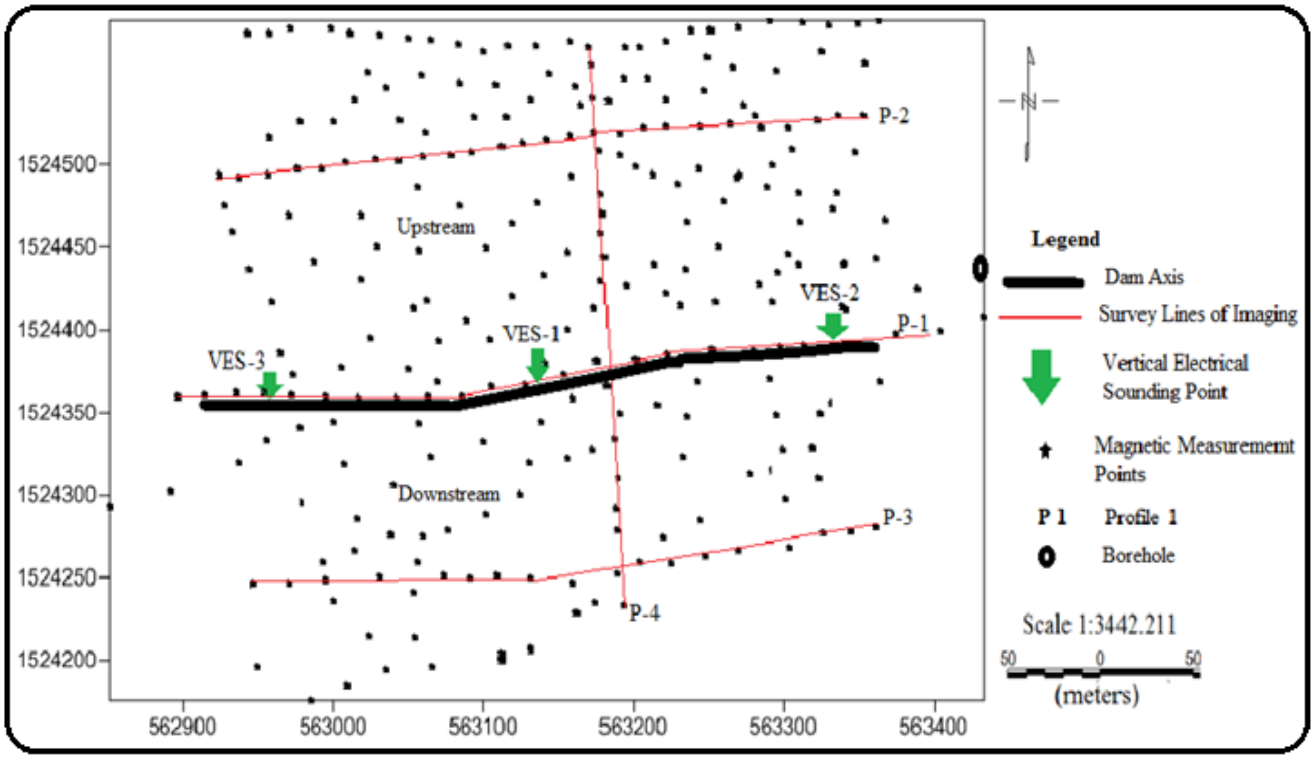

Figure 4.1 Location map of the geophysical survey traverses and random points.

The three parallel profiles are about 200m apart. The first profile (P_1) is exactly at the place where the dam foundation will be sited and it is surveyed by one main and two roll along sequences which covers a horizontal distance of 540m. The other two profiles P_2 and P_3, which are parallel to P_1, are positioned at upstream (in reservoir) area and downstream area of the dam axis respectively. While the forth profile (P_4) is oriented nearly perpendicular to the three profiles listed above. These three profiles P_2, P_3 and P_4 are surveyed by one main and one roll along sequences which covers a horizontal distance of 450m each. The main sequence contains 648 data points covering 360m horizontal distance while each of the roll along sequences contain 297 data points covering a horizontal distance of 90m. The setup of the instrument at the field is indicated in Figure 4.2.

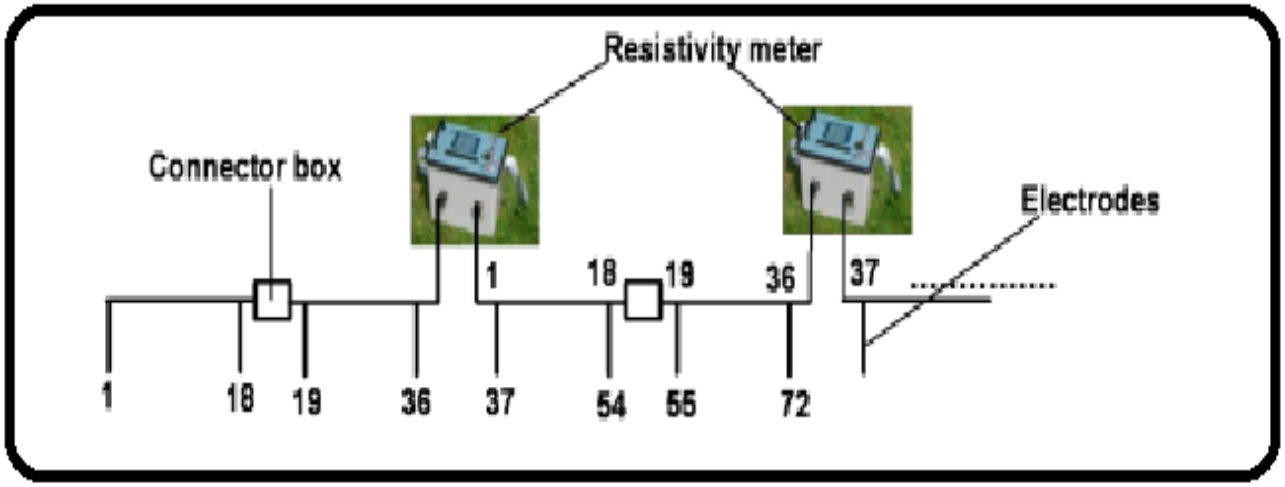

Figure 4.2 General field layout of 2D electrical imaging with the main (72 electrode layout) and the roll-along sequences (Hailemariam Siyum, 2011).

4.1.2 Vertical Electrical Sounding Data

Vertical Electrical Sounding survey was also conducted using IRIS SYSCAL R1 Plus Switch-72 instrument. Data were collected along four traverse lines in which three traverse lines (VES 1 , VES 2 and VES 3) are along profile one (P_1) of the 2D imaging at geographic coordinates of 563145E and 1524373N, 563341E and 1524380N and 562950E and 1524363N respectively. These VES points are E-W orientated with about 165m interspacing while the fourth traverse runs nearly perpendicular to these three traverses, which also corresponds to profile four (P_4) of the 2D imaging profile with N-S orientation. For all surveys, the maximum AB/2 distance covered at field is 220m. A measurement taken from field provides readings of induced current, respective

potential difference and calculated apparent resistivity of a point for predefined AB/2 and geometric factor. Location of the vertical electrical sounding points is shown above in Figure 4.1.

4.1.3 Magnetic Data

Magnetic data were collected using Proton Precision Magnetometer instrument. The surveying was stated by establishment of a base station within the study area at a place which is easily accessible and as far as possible from magnetic noise. In addition to the magnetic readings the geographic coordinates of the point at which the readings are taken is and the time of reading is recorded using Global Positioning System (GPS). Similar to that of the electrical resistivity data, magnetic data are collected along the predefined profile lines, which were used to conduct electrical resistivity surveys. In addition magnetic data are also collected randomly within and at the boundary of the study area. Magnetic data were collected from 124 data points with average spacing of 20m along the selected profile lines and at 140 data points for the random survey with average spacing of 30m. Therefore a total of 264 readings were collected during the field survey. At the field survey three magnetic readings were taken for a specific point and then average of this readings were used for the processing and interpretation purpose. The distribution of magnetic data in the study area is shown in Figure 4.1 above, and it is clear from the figure that the magnetic data are well distributed over the investigated area.

4.2 Data Processing

4.2.1 2D Electrical Resistivity Data Processing

The data generated at field from each main and roll along sequences are downloaded to a computer using the Prosys-II software. Then the data from each roll along sequence is added to the main sequence before the processing stage with the help of this software. After the summation, the summed data is filtered, by automatic filtering, and the noisy data is rejected. Finally the filtered data is saved in the Prosys-II software in ".dat" form and exported to RES2DINV software for processing. The filtered data, which is exported to RES2DINV software, is inverted by least-square inversion and with 5-7 iteration processes a representative earth model which would give similar subsurface apparent resistivity is produced for the purpose of analysis.

An automatic iteration process that fits the modeled data with the calculated one proceeds to analyze the data. A root mean square error (RMS) of the process was 5-8.8% and it was taken to be acceptable. The final output of RES2DINV software, the inverted 2D model resistivity section,

is the processing product of 2D survey (Figure 4.3). Finally such figures are used for interpretation purpose and to correlate the results of 2D imaging analysis with results of other methods.

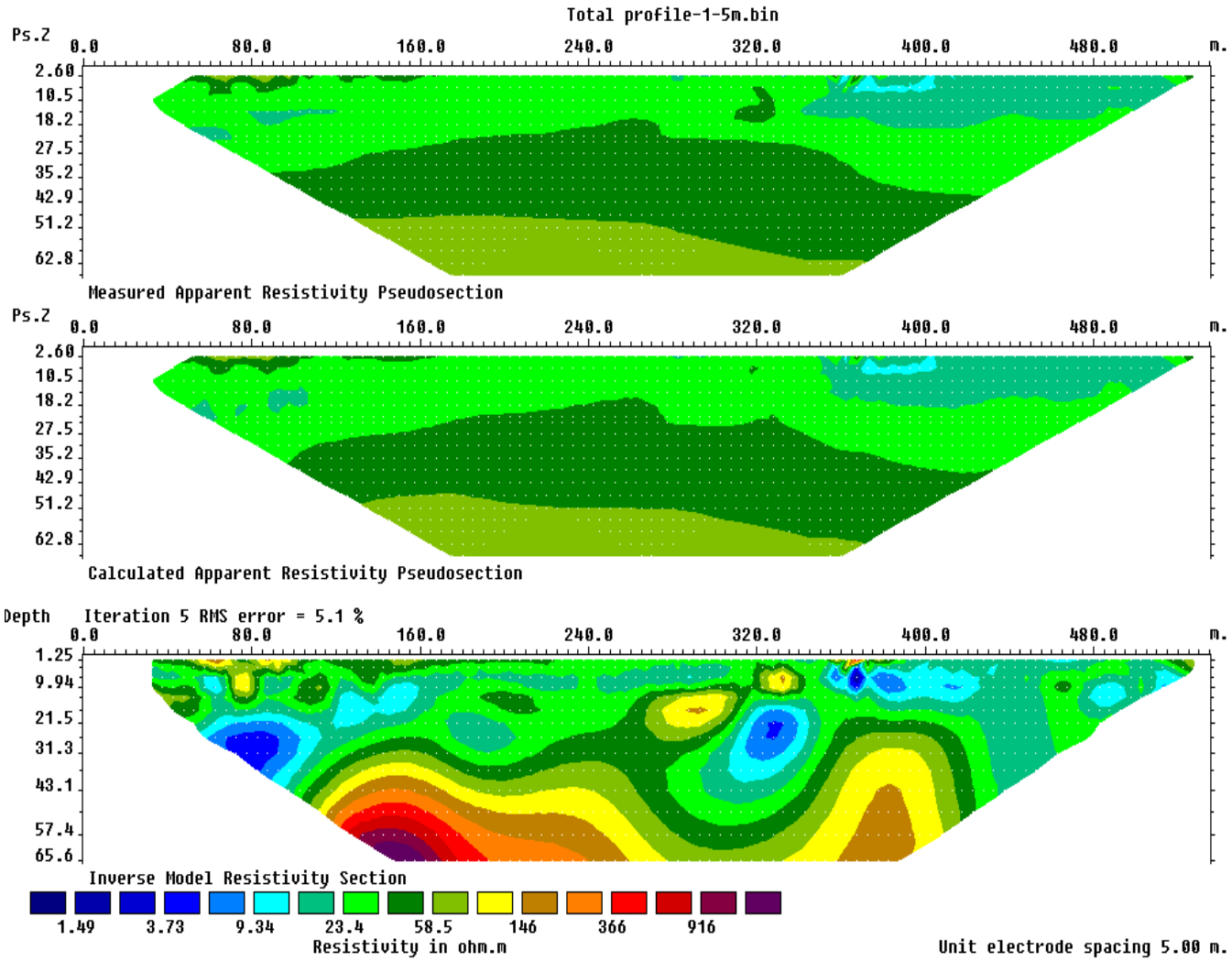

Figure 4.3 Measured, calculated and inverted 2D model resistivity section.

4.2.2 Vertical Electrical Sounding Data Processing

The vertical electrical sounding data is processed using RESIXIP and Win RESIST software and the maps are developed using Surfer and AutoCAD software. First the layer parameter are developed by processing the apparent resistivity data in RESIXIP software with the help of interactive graphics and by changing the model continuously, until a model that best fits to the curve is attained. Then the layer parameters and apparent resistivity values obtained from RESIXIP software are used for further processing using Win RESIST software to produce the interpreted resistivity curve that are displayed in Figure 4.4.

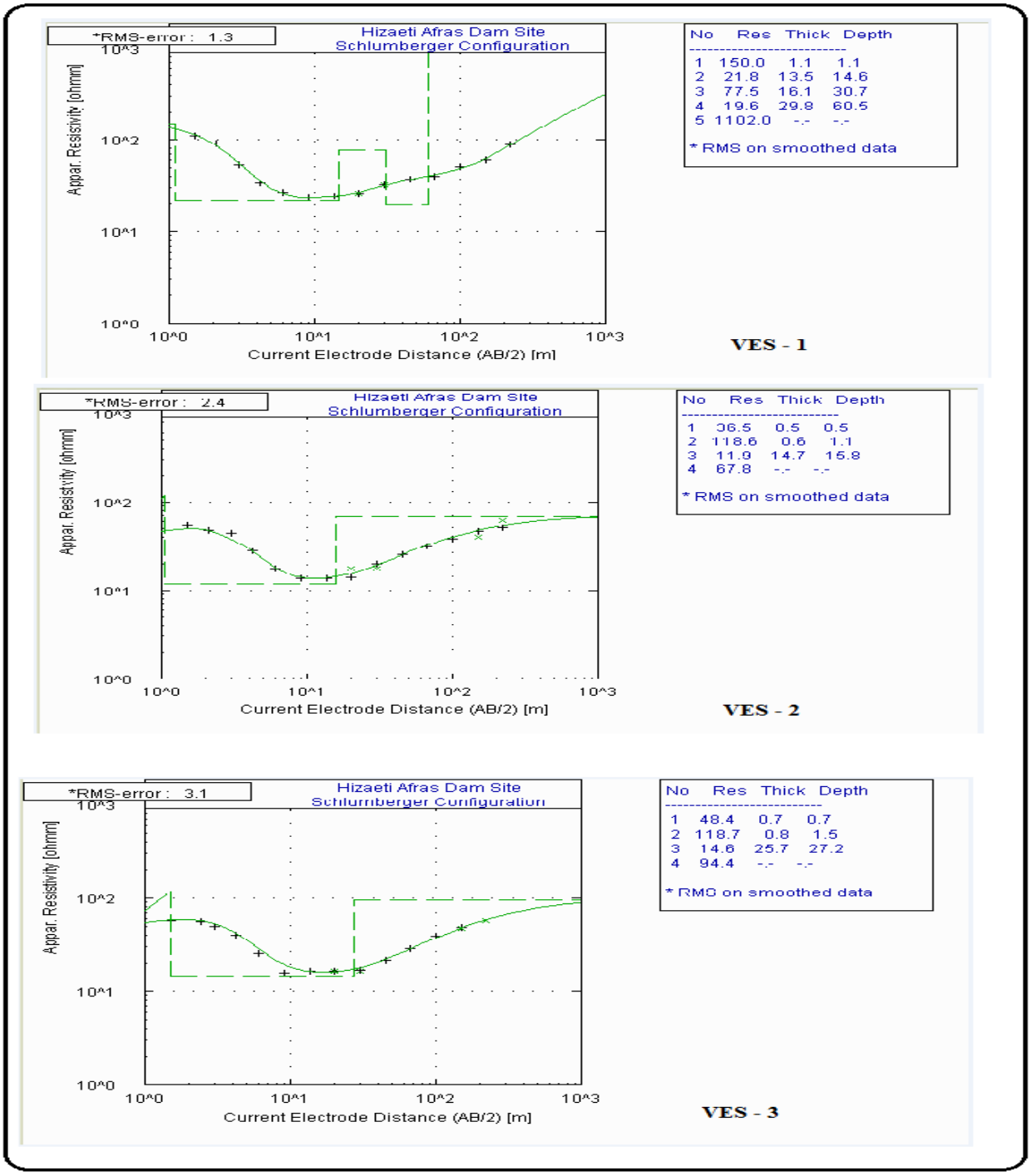

Figure 4.4 Interpreted VES curves of the three sounding points.

It is seen from the interpreted figures that a very good correlation between the field data and the interpreted model sections are obtained for all the three VES points. This is attested by an RMS error of 1.3 to 3.1 obtained for the sounding data. In the three sounding curves, a 3 to 4 layer of the

subsurface is seen and it well represents the subsurface (with the AB/2 of 220 m used for the survey).

Furthermore, pseudo-depth section map is developed using Surfer software from the apparent resistivity collected at field (raw data) and the distance between the measure points and geo-electric section map is constructed with the help of AutoCAD using the layer parameters generated by RESIXIP software for the three vertical electrical sounding points.

4.2.3 Magnetic Data Processing

For the purpose of diurnal correction the magnetic data collected at field was recorded in Microsoft excel. Using this software the diurnal variation of each point was calculated based on the reading of the base station. Then diurnal correction was done by subtracting the diurnal variation of each reading point from the reading taken by Proton Precision Magnetometer at that specific point.

In addition to the above correction the magnetic data required geomagnetic correction, which is a technique that removes the effect of geomagnetic references field from the survey data. The most accurate method of geomagnetic correction is the use of the International Geomagnetic Reference Field (IGRF) value (Kearey et al., 2002). Therefore, the correction was made using recent (2005) IGRF value for the study area obtained from Oasis Montaj of version 6.4.2. Finally the total magnetic field anomaly, obtained by subtracting the diurnal variation and IGRF values from the survey data, was used for processing to produce anomaly map, models and profile plots using Oasis Montaj and Microsoft excel software. Magnetic anomaly map of the area and profile plot of one traverse are displayed in Figures 4.5a and 4.5b. The average IGRF value used is 37231.

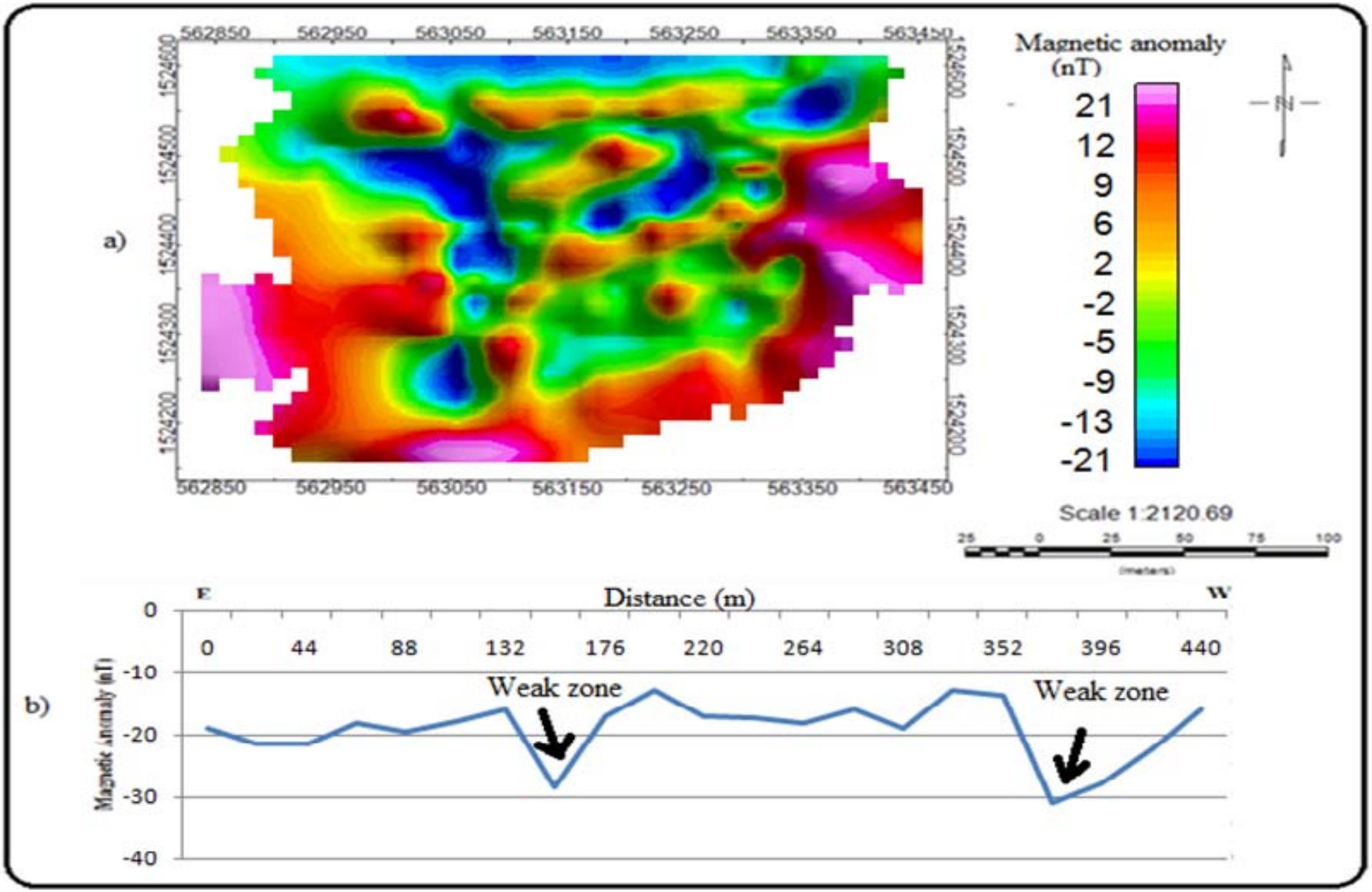

Figure 4.5 Magnetic anomaly map (a) and profile plot for survey line P1 (b).

CHAPTER - 5

INTERPRETATION

5.1 Introduction

Interpretation is made based on integration of results from the 2D electrical imaging, vertical electrical sounding, magnetic, and a borehole log data. A borehole dug at the boundary of the study area by Tigray Water Works Construction Enterprise for water supply purpose to Sheba Tannery S.Co was used to assist in the interpretation of the data. The total depth of the borehole is 78.5m while the depth of investigation of the 2D electrical imaging is 65m so that, the correlation is made only for the 65m depth. Furthermore, a correlation between the inverse model resistivity section and the magnetic anomaly profile plot, which is surveyed along the same survey line with the 2D electrical imaging, is done.

This chapter also includes interpretation of apparent resistivity sliced-stacked depth map, pseudodepth section map, geo-electric section, magnetic anomaly map, analytical signal map, tilt derivative map, Euler depth map and 2D magnetic model which are developed using different geophysical plotting software. The detailed interpretation of the study goes as follows:-

5.2 Profile-1

Profile one (P1) is aligned in a near E-W directon and runs over the place exactly where the dam foundation will be constructed. On this profile, electrical imaging data were collected from 1242 data points, which covers 540m horizontal distance. However, after filtering the noisy data only 1225 data points were used for the inversion purpose.

The least square inversion, done using RES2DINV software, resulted a good quality inversion model section (Figure 5.1b) with RMS error of 5.1% after five iteration processes, showing a good data quality. This inversion model is classified into three layers based on the information from the borehole log data; and it is correlated with the magnetic anomaly profile plot constructed from the data collected along the same profile (Figure 5.1a).

The first layer which extends up to 9m depth has intermediate apparent resistivity value that ranges from 58-146 Ωm. This resistivity value is the response of the top layer which is dominated by river deposits. The resistivity variations are the results of variable moisture content and

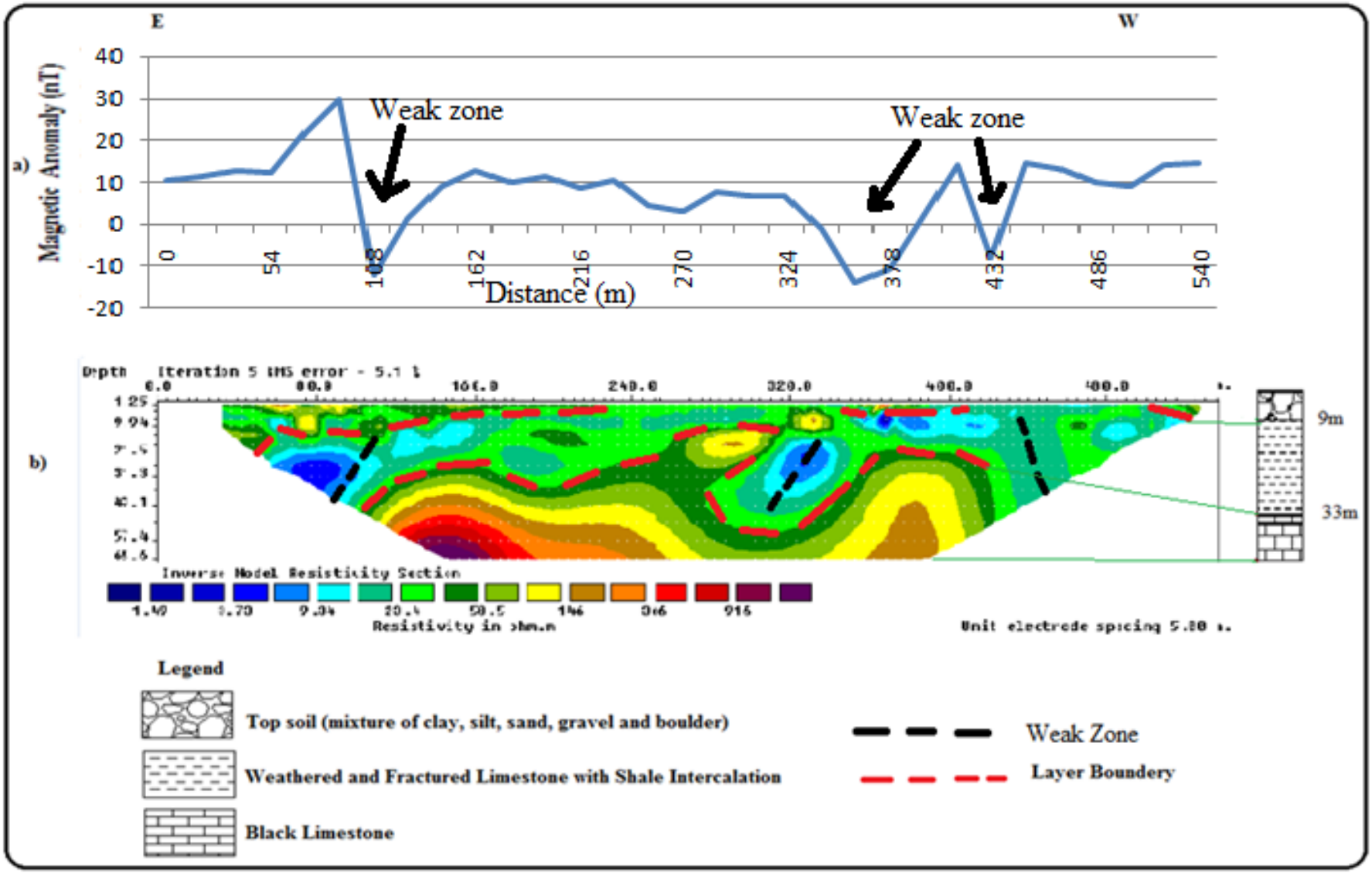

Figure 5.1 Interpretation of geophysical data of profile 1 a) magnetic anomaly profile plot and b) 2D inversion model resistivity section.

differences in lithology of the top soil. In some localities the loose sediments, which include sand and gravel, has developed ground contact problem during investigation, so as leading to this higher apparent resistivity value. This layer is thick at the eastern side and its thickness decreases gradually as going to western end part of the study area.

The second layer extends on average up to 33m depth and has an apparent resistivity value ranging from 1 Ωm to 23 Ωm. This lower resistivity value is due to the weathered and fractured limestone, which is considered as water bearing formation in the well completion report of the drilling enterprise. Contrary to the upper layer, it gets thicker at the western part of the study area while it is thin on the eastern part. This layer goes deeper at two distinct localities, which are at distance of about 100m and 435m from the eastern part. These two areas show structural discontinuities probably faults.

The third layer has higher apparent resistivity values ranging from 60 Ωm to 900 Ωm. This higher apparent resistivity value is a response of the competent rock, black limestone. The depth from surface to this competent rock varies on average from 20m to 33m.

The amplitude of magnetic anomaly profile (Figure 5.1a) conducted along profile one show condiderable variation in the upper and lower peaks, which ranges form -12 to 30 nT at a distance of 108m, form -14 to 8 nT at a distance of 350m and from -8 to 14 nT at a distance of 430m from the eastern part of the study area.

These lower peaks depicted in the profile plot line indicates the presence of weak zones. Frtheremore, the location at which all the structures found in both, magnetic and electrical tomography, methods nearly coinsides.

5.3 Profile-2

Profile two is surveyed along E-W direction and lies within the resorvior area, which is on the up stream side of the dam. This profile covers a distance of 450m which is surveyed by one main and one rollalong sequences. Accourdingly, data was colledted from 945 data points, in which after filtering the noisy data only 900 data points were used for the inversion purpose.

The inversion model section of this profile (Figure 5.2b) is produced by least square inversion with the RES2DINV software having RMS error of 6%. The different segments of the inversion model section are grouped into three layers based on the information from the borehole log data

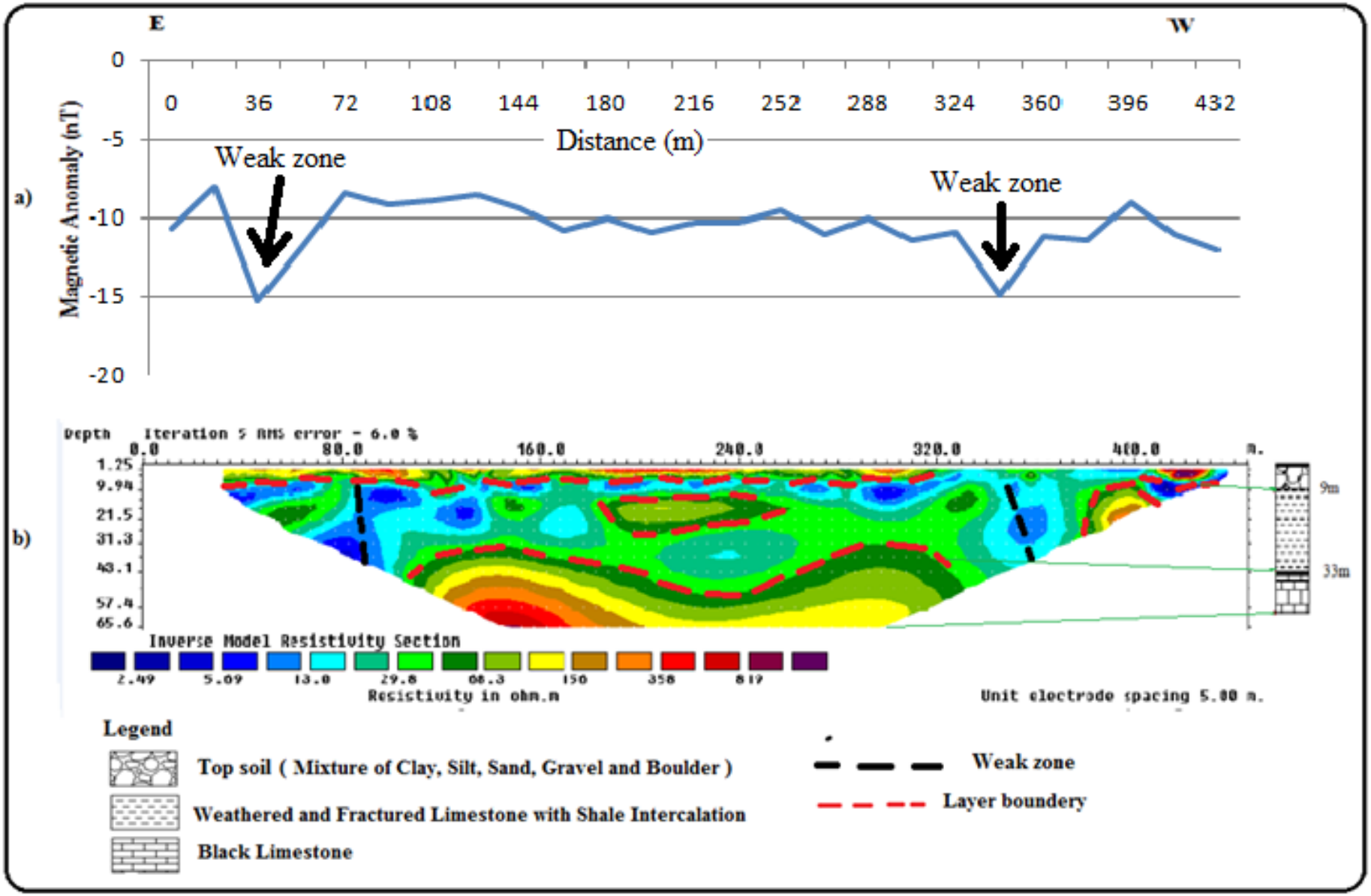

Figure 5.2 Interpretation of geophysical data of Profile 2 a) magnetic anomaly plot, and b) 2D inverse model resistivity section.

and it is correlated with the magnetic anomaly profile plot developed from a survey data conducted along the same survey line (Figure 5.2a)

According to the grouping, the upper geoelectric layer of this profile also extends nearly up to 9m depth. The apparent resistivity value of this layer ranges from 68-358 Ωm, which is the response of the top soil which is composed of river sediments dominated by silt and sand. This top layer has nearly uniform thickness starting from east up to 320m distance; however in the region between 320m-410m along the line, low resistivity responses of the top layer are recorded resulting from change in lithology of the upper surface.

The second layer which has an apparent resistivity value ranging from 2.5 Ωm to 29.8 Ωm extends up to 33m depth. This lower resistivity value is a response of the weathered and fractured limestone which is the main aquifer of the study area. This layer has greater thickness in the western part as compared with the eastern part of the study area. Similar to second layer of profile one, this layer extends to deeper part at two discrete localities, which are at distance of about 90m and 340m from the eastern part. These two specific areas indicate the presences of a structure.

The third layer of this profile has higher apparent resistivity values ranging from 68.3 – 819 Ωm. This high apparent resistivity value is a response of the hard black limestone which is exposed at different depths ranging from 25m to 35m. This competent rock is found at shallower depth on the eastern part of the study area which is similar to the case in profile one.

The amplitude variation of magnetic anomaly profile (Figure 5.2a) conducted along profile two ranges nearly form -15 to -7 nT in both locations. These lower peaks, which indicate the presence of weak zone, appear at a distance of about 40m and 340m from the east to the west direction of the survey line. Therefore, they almost coincides with the discontinuites depicted on the 2D inversion model section of this profile.

5.4 Profile-3

Profile three was condacted on the downstream side of the dam foundation along similar orientation with the above two profiles and it covers a distance of 450m. Out of the data collected from 945 data points only 923 data points were used for the inversion purpose. The least square inversion of this data resulted in a good quality inversion model section (Figure 5.3b) with RMS error of 3.9%. Analogous to the above two profiles, the different segments of the inversion model

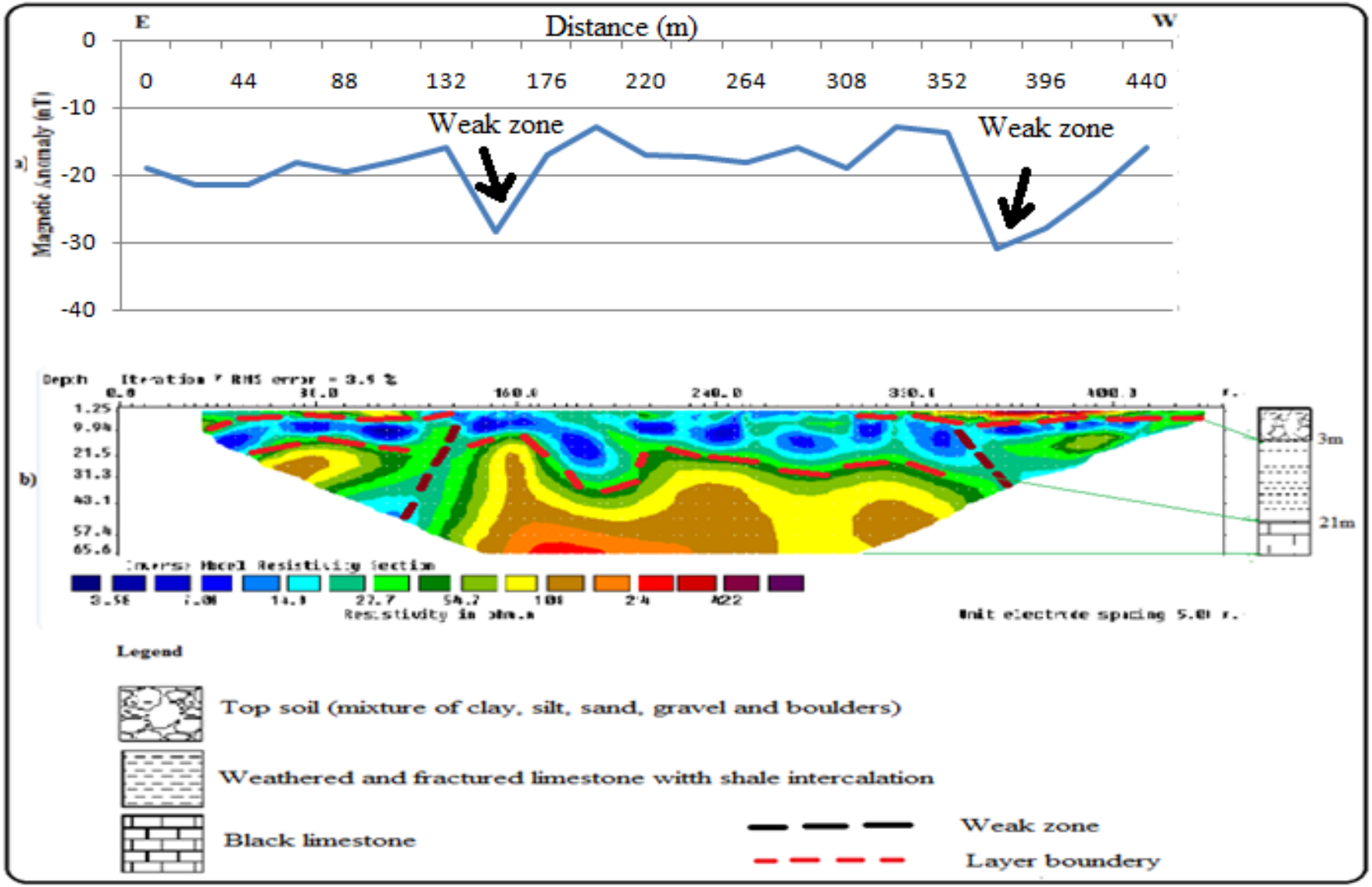

Figure 5.3 Interpretation of geophysical data of profile 3 a) magnetic anomaly curve, b) 2D inversion model section

section are clustered into three layers. And it is correlated with the magnetic anomaly profile plot developed from survey data conducted along similar survey line, profile three (Figure 5.3a).

Thus, the upper layer of this profile is very thin in thickness which is not more than 3m and it shows lateral variation along the survey line. This layer has apparent resistivity value which ranges from 54-214 Ωm as a response of the lose sediments.

The second layer has an apparent resistivity value ranging from 3.6 Ωm to 27.7 Ωm. This lower resistivity value is a response of the weathered and fractured limestone with shale intercalation. Furthermore, the irrigation water used by local farmers to irrigate their land at the downstream side of the dam could have an effect to lower the apparent resistivity values. This layer extends to a depth of 21m and has nearly uniform thickness in the central part of the study area. In the same way to second layers of the above profiles, this layer extends to deeper part at two distinct localities, which are at distance of about 140m and 340m from the eastern part and this is due to structural discontinuities.

The third layer of this profile has higher apparent resistivity values ranging from 54.7 Ωm to 422 Ωm. This high apparent resistivity value is a response of the black limestone rock in which its upper surface is exposed at depths ranging from 15m to 21m. Similar to the above two profiles this sound rock is found at relative shallow depth in the eastern part of the study.

The amplitude of magnetic anomaly profile (Figure 5.3a) conducted along Profile three varies form -28 to -16 nT at a distance of 160 m from east and form -31 to -12 nT at a distance of 360m from east. The lower peaks that appered at a distance of about 160m and 360m from the east indicates the presence of weak zone at that specific localtion. Thus these two lower peak which indicate the presence of weak zone nearly conside with the discontinuites of the 2D inversion model section of this profiel.

5.5 Profile-4

This profile is surveyed in N-S direction which is perpendicular to the above three survey traverses. It cuts the above three profile which run E–W direction. And it is surveyed to check whether there are structures/weak zones that run parallel to the dam axis and to visualize the lithological stratification in the N-S direction.

The surveyed profile has a length of about 450m and on this profile data was collected from 945 data points. However, after filtering and removing the noisy data only 884 data points were used

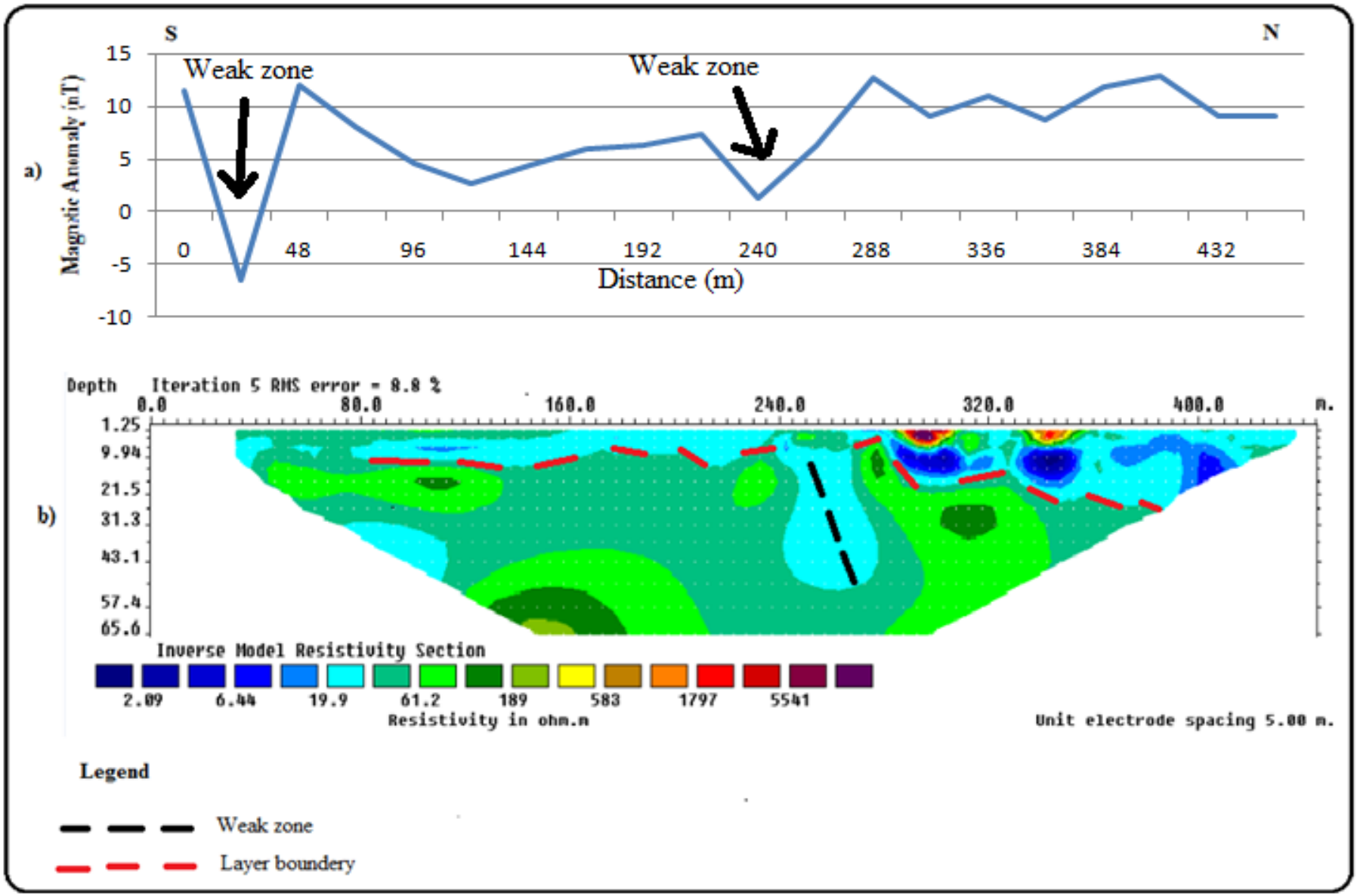

Figure 5.4 Interpretation of geophysical data of profile 4 a) magnetic anomaly curve, b) 2D inversion model section

for the inversion purpose, number of data points believed to give a high resolution image of the ground. The inverse model resistivity section (Figure 5.4b) produced by the least square inversion of the collected row data has RMS error of 8.8%.

The inverted 2D model section of this profile is conveniently divided into two layers, and it is presented along with the magnetic anomaly profile plot surveyed along the same survey line which runs in the N–S direction (Figure 5.4a).

The inverse model resistivity section for this line is distinct from the lines that run parallel to the dam axis, i.e. profiles 1, 2 and 3, in that it shows only two layers. On this profile, the first layer is dominated by very low resistivity response, 2.09 Ωm -19.9 Ωm, with clear lateral variation in resistivity along the line.

A relatively higher resistivity response of the top layer is obtained in the region around 280m and 340m from the eastern end of the study line where the apparent resistivity of this layer ranges from 189 Ωm to 1797 Ωm. Similar to that of profile two, there was a ground contact problem while conducting the roll along sequence of this profile due to the loose sand and silt which act as bad galvanic contact areas requiring higher input voltage from the instrument. Therefore this very high resistivity region within the top layer, which is in the northern part of the survey, is the response of these loose sediments. This layer extends to about 21m in the northern end of the survey line whereas it has less than 9m depth extent on the southern end.

The second layer which is exposed at shallow depth on the southern part of the survey line, relative to the north, possess apparent resistivity values ranging from 61.2 Ωm to189 Ωm. it is observed from the above three parallel profile that the black limestone is situated at shallow depth in the southern part of the survey area and it goes to greater depth in the north. Furthermore, the apparent resistivity of the black limestone is also similar to this range. Therefore, this apparent resistivity value range is interpreted as the response of the competent rock, black limestone. As it can be visualized from the model the black limestone is found at shallow depth in the downstream side of the dam axis which is most preferable to construct a dam on it.

The 2D inversion model shows the presence of weak zone at distance of 240m from the south. This weak zone is filled by a material with very low resistivity value, probably from the first layer.

The amplitude of magnetic anomaly profile (Figure 5.4a) surveyed along similar survey line with Profile 4 varies form -6 to 12 nT at a distance of 30m from south and form 1 to 14 nT at a distance of 240m from south. These two lower peaks possibly indicate the presence of weak zones at a distance of about 30m and 240m from the south. The weak zone that appeared around 30m is not visible in the inverted model of 2D. howevere, the one that appeared around 240m consides with the weak zone of the 2D inversion model.

5.6 Correlation of the 2D inversion model sections

It is advisable to combine the three surveyed profiles as in Figure 5.5 for better understanding and visualization of the subsurface condition in the study area. These three profiles are parallel to the dam axis as well as to each other and the survey was conducted from the east to west direction.

The point where survey for profile-1, the traverse line that runs along the intended dam axis, started is 90m ahead of the starting point of the other two profiles which were conducted upstream and downstream side of the dam axis. This is because there was a physical barrier (a school) on the upstream side and the river cutting on the downstream side, which did not allow starting the survey from equal point on the eastern side. However, all the three profile have parallel end point at the western part of the study area.

As it can be visualized from the Figure 5.5, the first layer with high apparent resistivity value is relatively thick in the eastern part of the study area in almost all the profiles with a decreasing coverage from upstream to downstream side. And the thickness of the second layer is significant in the western part as compared to the east in all the profiles. However, the thickness of this layer also considerably decreases on the downstream side as compared to the upstream side of the dam axis.

The third layer has undulating nature in all profiles and it is exposed at shallow depth in the eastern part of the area relative to the western part. This layer is also found at shallow depth (15m) on profile three with comparative to the other profiles.

The apparent resistivity values of the first layer ranges from 54 Ωm to 358 Ωm in all the profiles. Similarly the apparent resistivity values of the second and third layers ranges from, 1 Ωm to 30 Ωm and from, 54 Ωm to 900 Ωm respectively in all the profiles.

The correlation of these 2D inversion model sections shows that the depth to the sound foundation is relatively shallow depth in the downstream side of the dam axis and on the eastern part of the

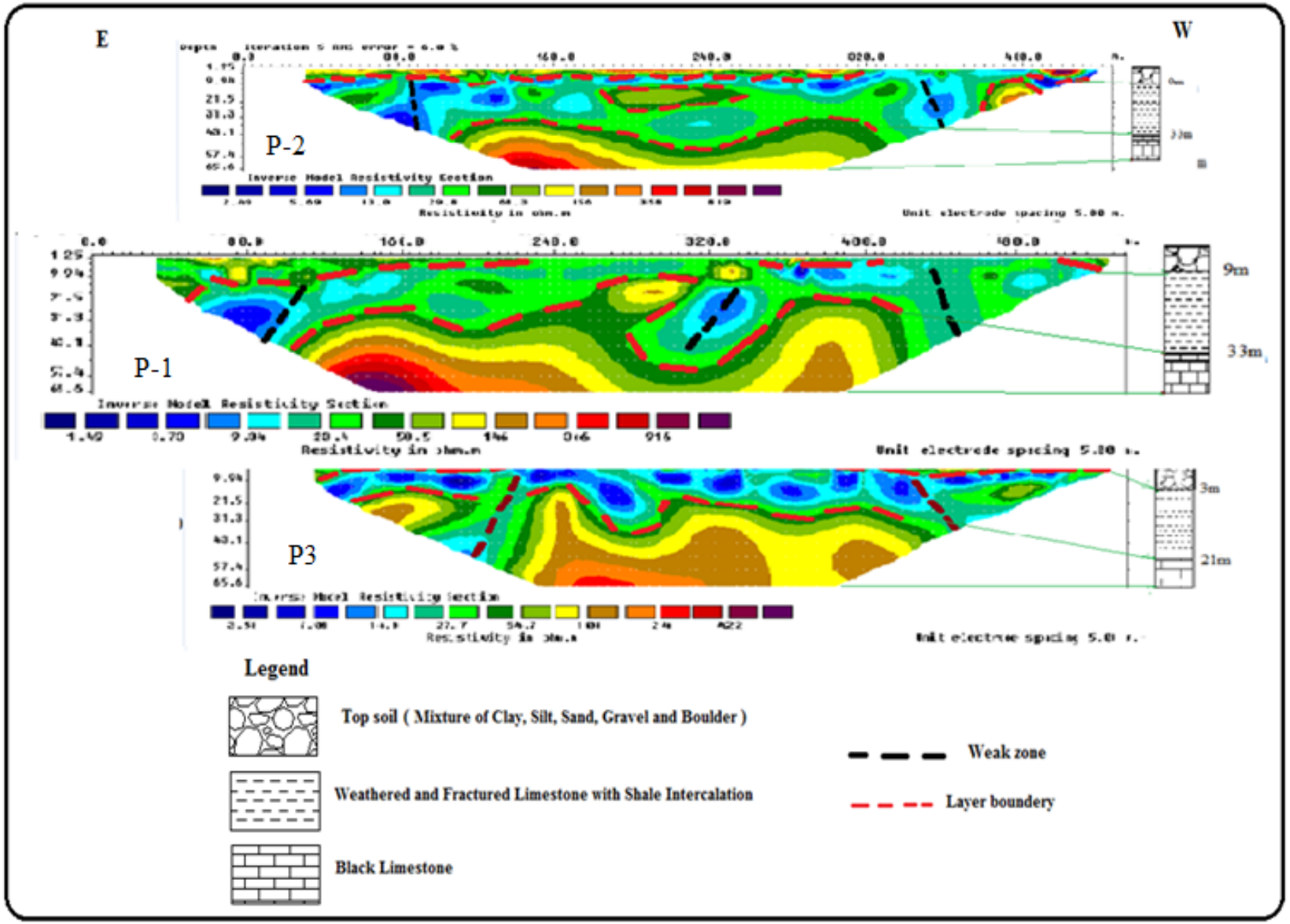

Figure 5.5 Correlation of the 2D inverse model resistivity sections.

study area. on the contrary the material which poor for foundation purpose is thicker in the northern and western side of the surveyed area.

Furthermore Figure 5.5 shows the existence of a weak zone, probably a fault line that cuts all the profiles at nearly equal point which is around 100-110m from the western side of the study area and this is the place where the existing dam failed through. In addition there is another structure that cut the three profiles around 120m – 160m from the eastern part of the study area.

5.7 Apparent Resistivity Sliced–Stacked Depth Map

The sliced–stacked depth map of apparent resistivity (Figure 5.6) was prepared at selected depth from the 2D electrical imaging data and this aid to visualize clearly the apparent resistivity distribution of the survey all over the surveyed area laterally and vertically. This map helps to understand the subsurface geological variation in lateral and vertical directions.

The developed sliced–stacked depth map shows that, at 2m depth a geological formation with very low apparent resistivity covering the entire surface. However, with increasing depth it depicts a clear zoning in resistivity variations both horizontally and vertically. Accordingly the study area is subdivided into three zones (zone I, zone II and zone III).

Zone-I is the area with very low apparent resistivity value ranging from 10 Ωm to 90 Ωm and it is expected to be the response of the weathered and fractured limestone. This zone starts at 2m depth and extends up to 47m depth covering most of the western part of the study area specially the north western portion. In addition, it also has a considerable coverage in the northeastern part of the study area which extends up to the depth of 35m. However, the extent of coverage in both locations gradually decreases with depth.

Zone-II is described by relatively intermediate apparent resistivity value ranging from 110 Ωm to 190 Ωm which is likely to be the response of weathered and fractured limestone with shale intercalation. This zone covers most of the central part of the study area starting from 10m up to 47m and its coverage increases with depth.

Zone-III is characterized by relatively very high apparent resistivity value which ranges from 210 Ωm to 290 Ωm. This high resistivity value is possibly the response of the competent black limestone formation. This formation starts at a depth of 10m in the southeastern part and increases its coverage with depth.

Generally this map shows that the western and northeastern part of the area comprises subsurface formation which has very low resistivity as a result of weathering and fracturing. Hence, it is not recommended for foundation purpose and/or it requires special attention in design and construction. However, most of the eastern and southern part is covered by a formation which has intermediate to high resistivity value. This higher resistivity values are the responses of relatively harder formations as a result it will be advisable to construct the dam foundation in the southern part of the study area. This result is similar with the results drawn from the 2D inverse model resistivity section.

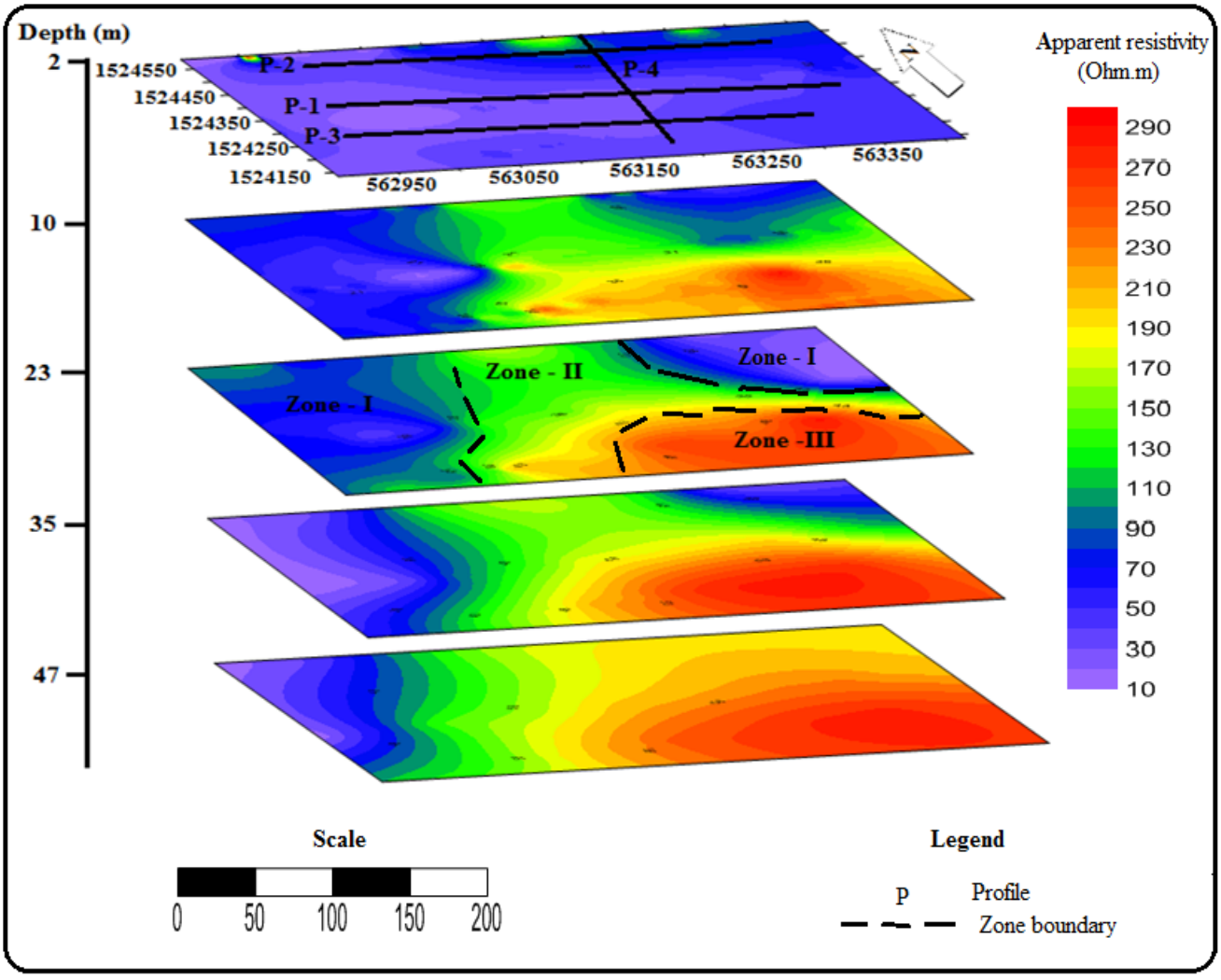

Fig 5.6 Apparent resistivity sliced–stacked depth map of the survey area. The orientations of the profiles from which the data have b een extracted are shown on the top slice.

5.8 Electrical Resistivity sounding

As mentioned in the earlier sections vertical electrical sounding data were collected at three sounding points all lying along the proposed dam axis (Figure 4.1). The VES points are spaced at about 165 m spacing and have been conducted with half current electrode spacing (AB/2) of 220 m. The individual VES are interpreted to get the layer parameters (resistivity and thickness of the subsurface layers) as given in Figure 4.4.

The VES data are presented in the form of apparent resistivity pseudo depth sections and geoelectric section and discussed separately in the following sections.

5.8.1 Pseudo-Depth Section Map

The apparent resistivity pseudodepth section (Figure 5.7) is prepared from the VES surveys carried out along Profile-1, which is the place where the dam foundation will rest. Pseudodepth maps that are prepared by taking raw resistivity data show resistivity variation of the subsurface both in lateral and vertical directions without introducing the bias of data filtering and interpretation software.

Accordingly the map (Figure 5.7) indicates that the top most part of the study area has higher resistivity value that ranges from 60Ωm to 110Ωm. This is expected to be the response of the top soil composed of the mixture of clay, silt, sand, gravel and boulders derived by river action. Furthermore similar resistivity values are also shown starting from 100m depth and covering most of the area below VES–1 and VES–2. However, the cause for this response could be the black limestone, as indicated in the inverted model section and the sliced depth map.

Similar to that of the sliced stacked depth map of the 2D electrical imaging, this pseudodepth map shows that the western parts of the study area have very low resistivity value for considerable depth while the low resistivity in the eastern pare has limited depth. In addition to these two localities there is also a low resistivity area right beneath VES – 1. These areas have a resistivity value ranging from 10Ωm to 30Ωm and this is could be the response of the water saturated weathered and fractured limestone.

An intermediate resistivity value ranging from 40 Ωm to 70 Ωm covers the area at shallow depth beneath VES – 1 and VES – 2. This intermediate resistivity value is the response of the weathered and fractured limestone with shale intercalation. The same phenomenon has also observed in the sliced depth map of the 2D electrical imaging.

In the pseudo-depth map there is a distinct lateral resistivity variation at depth between VES – 1 and VES – 2 as indicated in the map by dashed lines. This lateral resistivity variation could be the response of a structure.

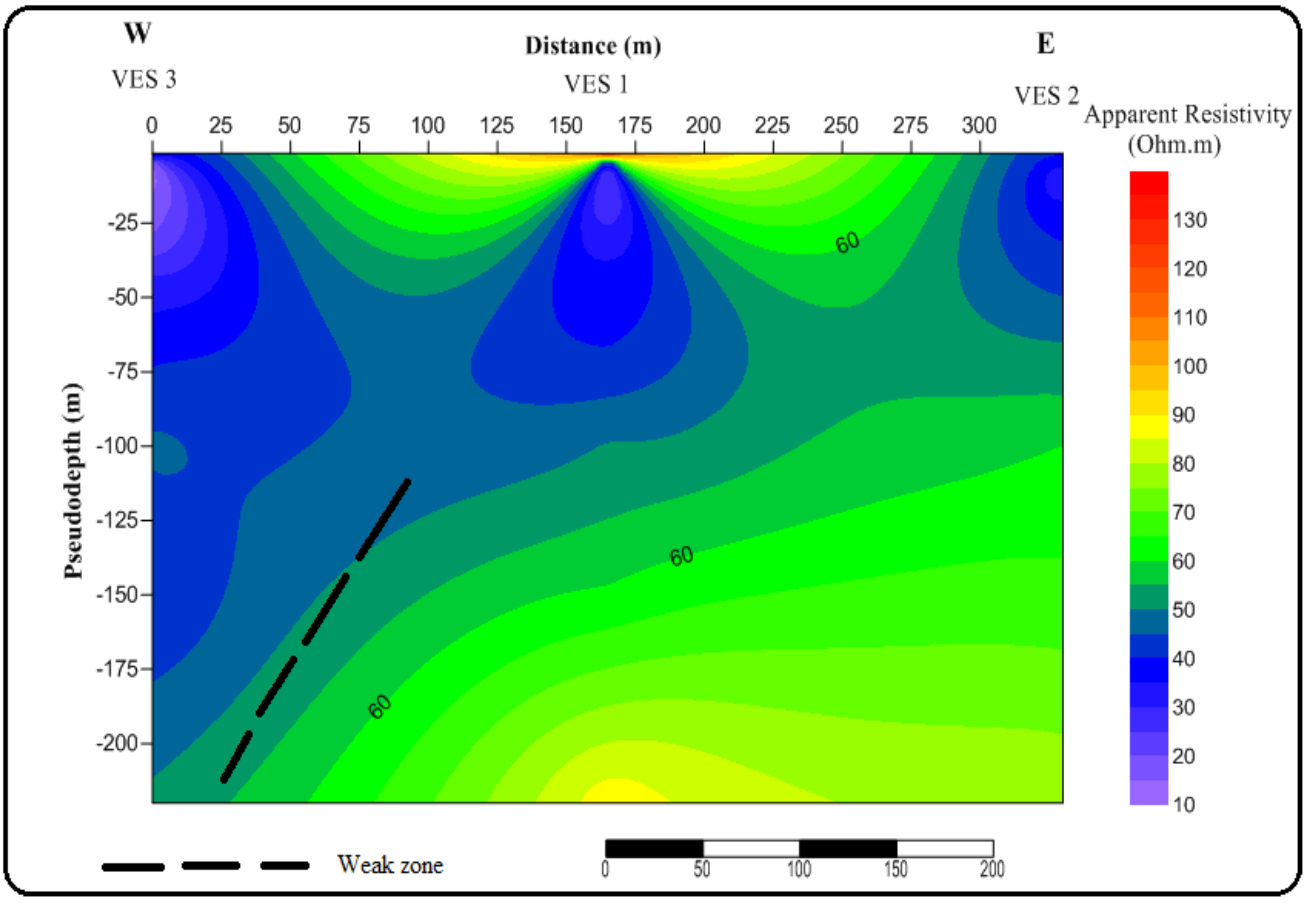

Fig 5.7 Apparent resistivity pseudodepth section map of the VES line that runs along the proposed dam axis.

5.8.2 Geoelectric Section

The geoelectric section (Figure 5.8) is constructed from the interpreted resistivity and depth values of the three VES conducted along profile-1. The layer mapped at the top has a resistivity value ranging from 103 Ωm to 150 Ωm. This is due to the top soil, which includes clay, silt, sand, gravel and boulder.

The second layer, which is over lain by the top soil, has resistivity value ranging from 12 Ωm to 22 Ωm. This low resistivity value is the response of the water saturated weathered and fractured

limestone. This layer is considered as an aquifer by the Tigray Water Works Enterprise, who has drilled a shallow well at and around the study area. The differential subsidence of this layer to greater depth on western part of the study area could be due to a discontinuity that has revealed in the pseudo-depth map above. This layer extends in depth from 16m in the east to 28m in the west.

The third layer possesses an apparent resistivity value ranging from 68 Ωm to 94 Ωm which could be the response of the black limestone formation. This formation is exposed at shallow depth (at about 16m) in the eastern part of the study area while the depth of exposure of this unit in the western part goes up to 28m.

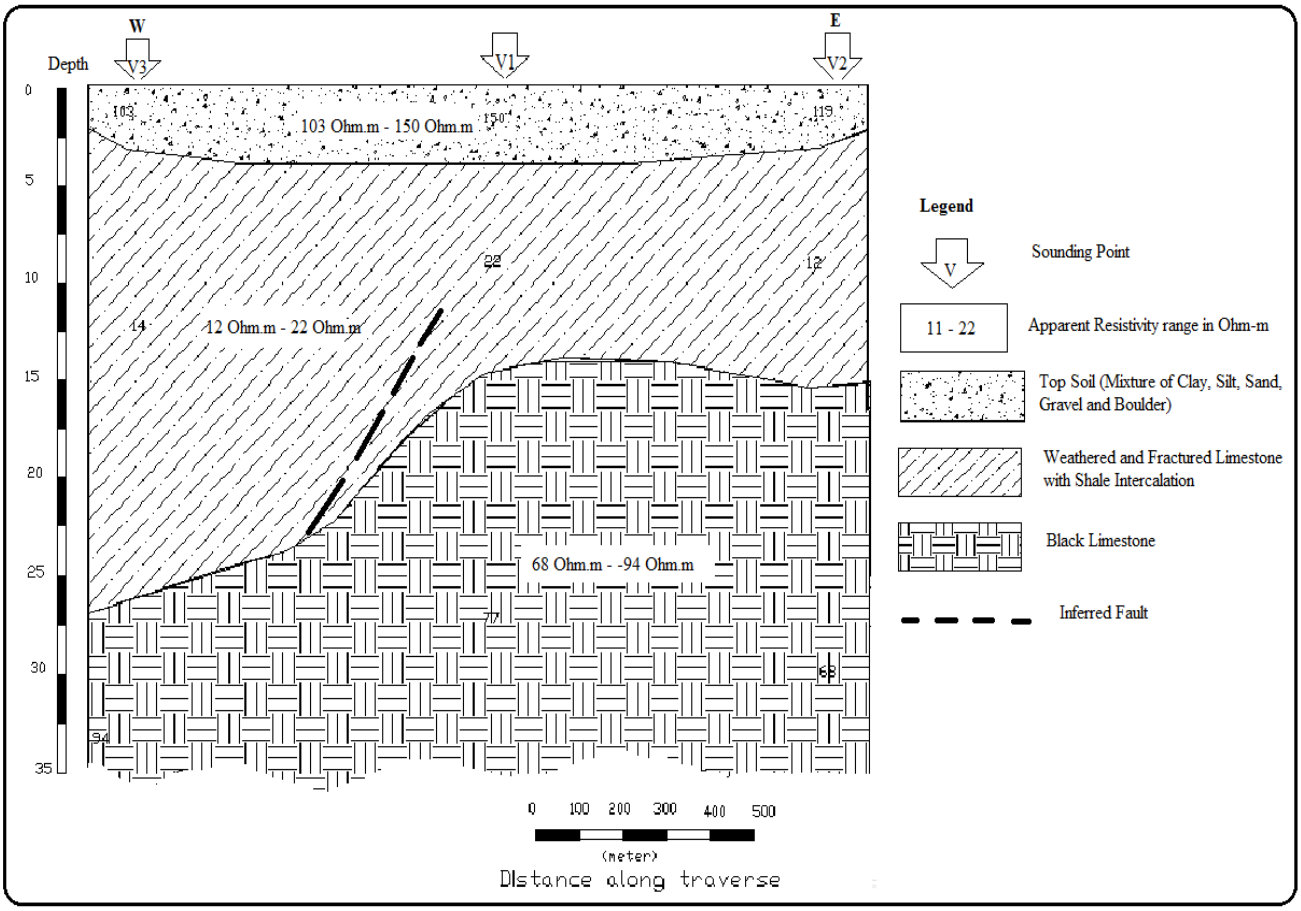

Fig 5.8 Geo-electric section map

5.9 Magnetic Anomaly Map

One of greatest application of magnetic method in engineering studies is to locate boundaries between different lithologic units and geological structures that display magnetic contrasts such as faults or dykes. To interpret the magnetic data in terms of such subsurface indications, the magnetic data are presented in different forms. After applying all the necessary reductions, the

magnetic anomaly map is prepared as shown in Figure 5.9. According to this map the study area is classified in to three zones. Zone-I is characterized by very higher magnetic anomaly and it covers the southwestern, the southern and southeastern part of the study area.

Zone-II, which have intermediate magnetic anomaly covers most of the central part of the study area. The area designated by Zone-III show very low magnetic anomaly and it covers the northern and some portion of the central part of the area. Moreover, this zone show N-S trend on the western part of the survey area. This N-S trending zone with low magnetic anomaly is interpreted as weak zone on the analytical signal and tilt angle derivative maps. Furthermore, two possible weak zones, with E-W and NE-SW trend, are also indicated on the map.

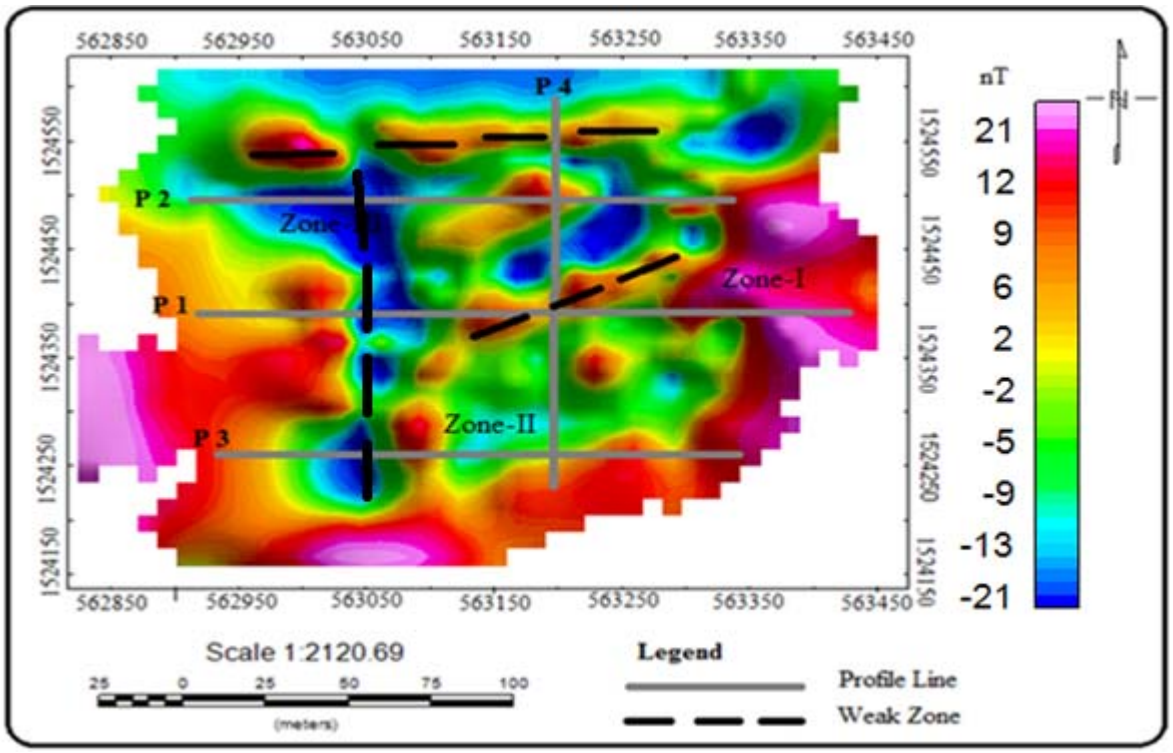

Figure 5.9 Magnetic anomaly map of the survey area.

5.10 Analytical Signal Map

As it is displayed in Figure 5.10, analytical signal map is developed from the magnetic data collected at field. Since analytical signal map shows the response of anomalous bodies from their upper portions, it is very help full to visualize the near surface conditions. Furthermore the analytic signal map shows maximum contrast over magnetic contacts. Accordingly, there are four distinct and aligned weak zones in the surveyed area. As indicated on the map one of the weak

zones is near parallel to the dam axis while the others have N-S, NE-SW and NW-SE trend and all these have a possibility of crossing the dam axis.

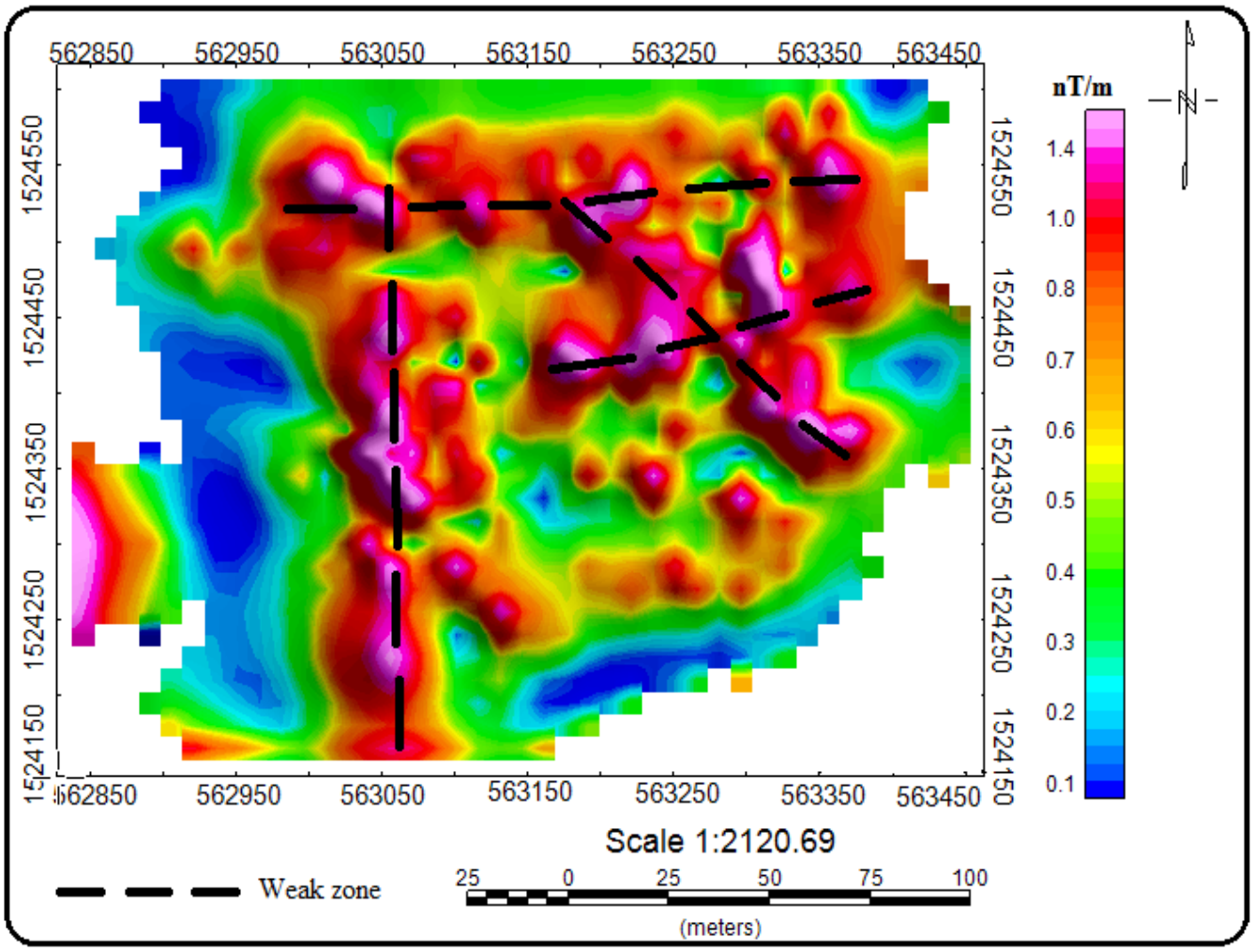

Fig 5.10 Analytical signal map of the surveyed area.

5.11-The Tilt Angle Derivative

Tilt angle is capable of edge detection and delineation of source body orientation. It produces a zero value over or near the source edges with positive values over the source and negative values outside the source. Accordingly the tilt angle map (fig 5.11) shows the orientation and relative position of the weak zones in the surveyed area clearly as it is demarcated on the map. The orientation and position of the weak zones indicated in the tilt angle map is consistent with analytical signal map discussed above.

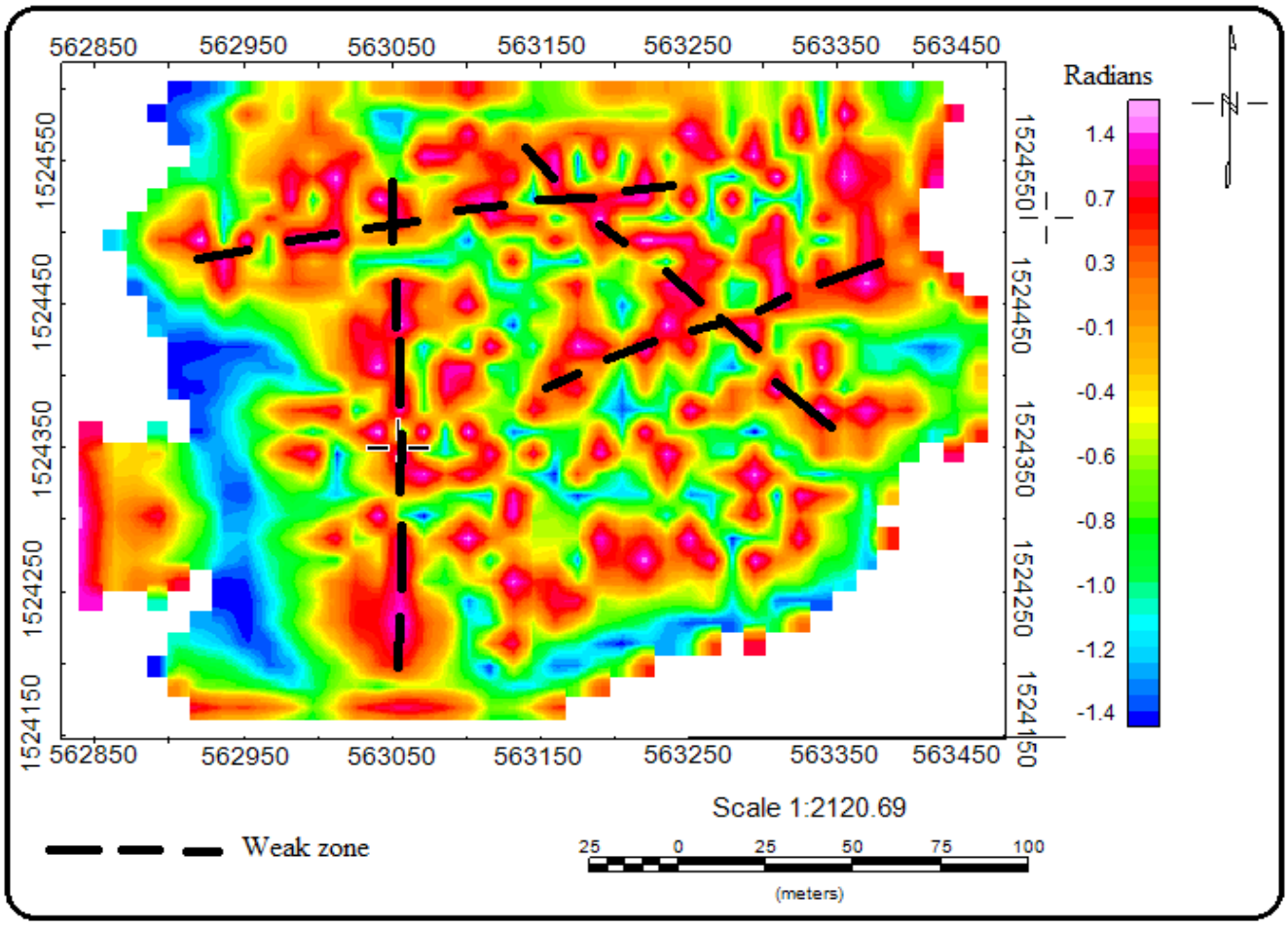

Figure 5.11 Tilt angle derivative map of the surveyed area.

5.12 The Euler Deconvolution

The Euler deconvolution method is a quasi-automated interpretation method often used for estimating depth and delineating boundaries of anomalous bodies. The most critical parameter in the Euler deconvolution is the structural index, η. This is a homogeneity factor relating the magnetic field and its gradient components to the location of the source. essentially, η measures the rate of change of the fields with distance from the source and is directly related to the source dimension. A correct η gives the tightest clustering of the Euler solutions around the geologic structure of interest (Thompson, 1982; Reid et al., 1990). Thompson showed that Euler's equation could be written in the form

$$(x-x_o)\frac{\partial T}{\partial x}+(y-y_o)\frac{\partial T}{\partial y}+(z-z_o)\frac{\partial T}{\partial z}=\eta(B-T)$$

where (x_o, y_o, z_o) is the position of a magnetic source whose total field T is detected at (x, y, z).

the total field has a regional value of B and η is the structural index. Accordingly after repeated trials for different structural indexes, η, an Euler depth solution map with better clustering is obtained for structural index of 1.5 as shown in fig 5.12 from the magnetic data collected at field. Based on the Euler depth solution, the depth to the source body in the central part of the study area is from 9m to 15m whereas in the areas which are interpreted as weak zones the depth goes from 18m to 42m.

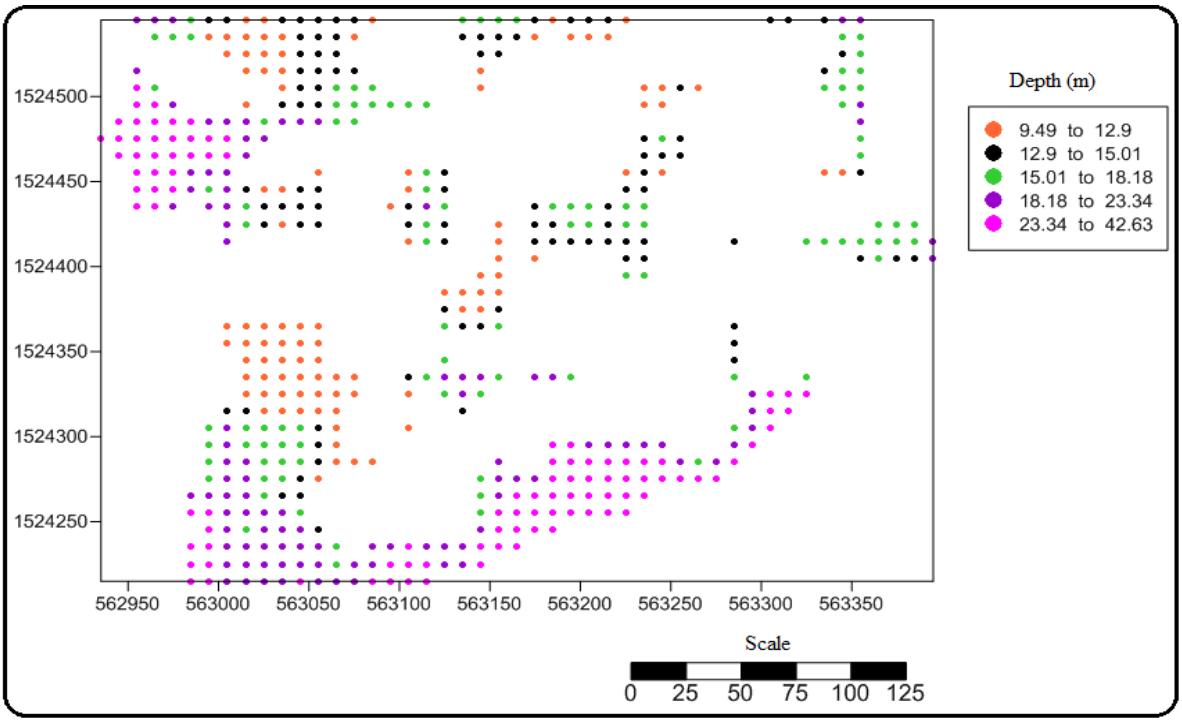

Fig 5.12 Euler depth solution map of the survey area.

5.13 2D profile modeling

Modeling is done using the GM-SYS modeling software. It is an interactive forward modeling program which calculates the magnetic response from a user defined hypothetical geological model. Any difference between the model response and the observed magnetic field are reduced by refining the model structure. It should be noted that magnetic models are non unique, i.e. many earth models can produce the same magnetic response, and similarly, several geological lithologies may be interpreted from a given model block's susceptibility properties. It is therefore importance to use as many independent source of information as possible to help constrain the model. The 2D model created by GM-SYS extends to depths of 50km by default and it changes

with depth (Z direction) and along the profile (X direction, perpendicular to strike) (GETECH Group plc, 2007).

Accordingly 2D magnetic modeling is developed along profile-1 from the analytical signal map as shown in Figure 5.10. This model is developed based on the information from the inverted model section of imaging, the geo-electric section of vertical electrical sounding and borehole data. The developed model has an error of 0.263 and it perfectly matches with all the maps and curves developed along profile from the different methods in displaying the layering, fault location and depth to the sound foundation. Based on this model, the faults are located around 140m and 420m from the west and the sound foundation is exposed at shallow depth, which is at about 19m, in the eastern part of the study area relative to the western part and this is consistent with all the maps and models discussed above.

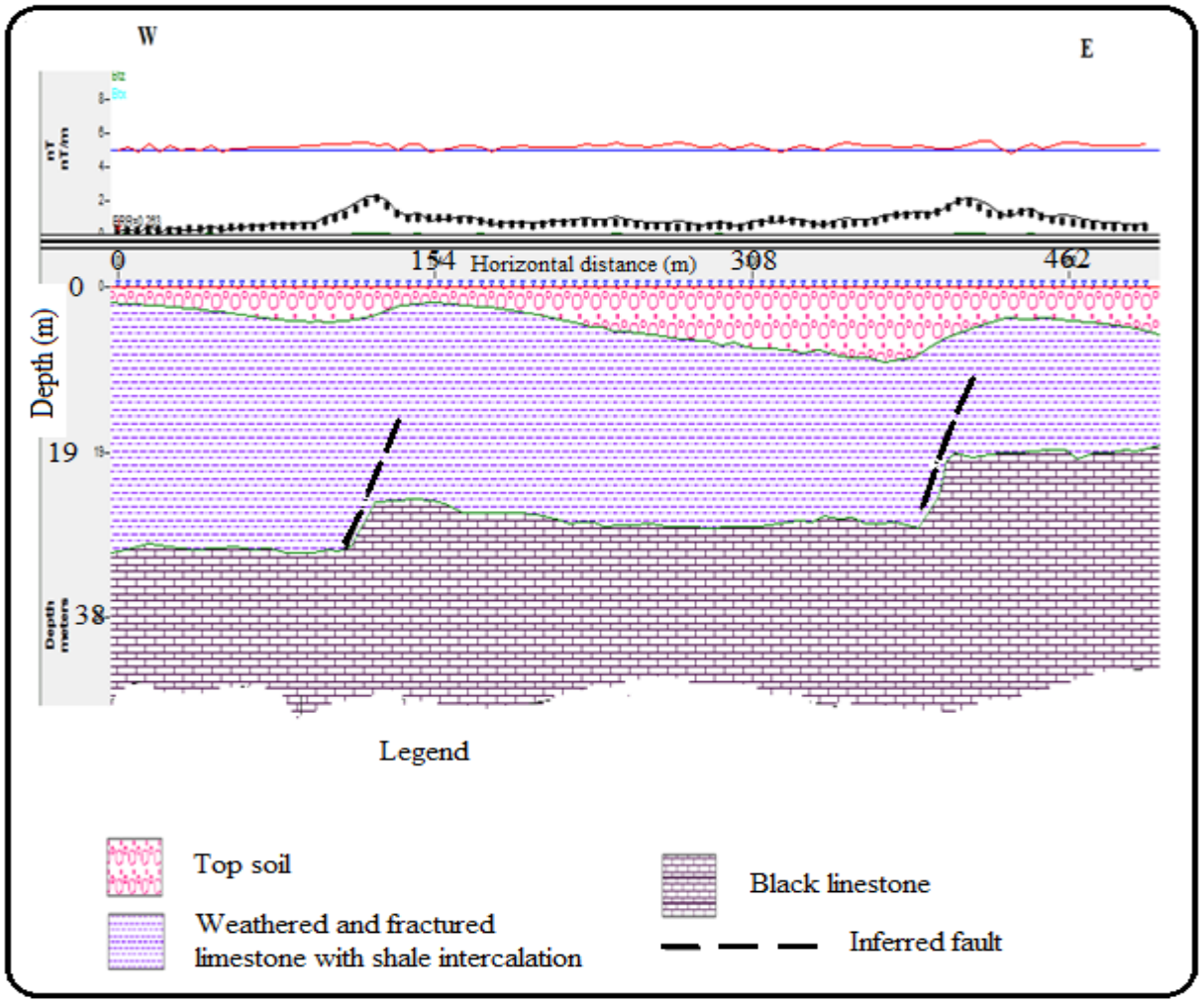

Figure 5.13 2D magnetic modeling along Profile-1.

CHAPTER - 6

CONCLUSION AND RECOMMENDATION

6.1 Conclusions

An integrated geophysical investigation for engineering site characterization of a dam construction site has been conducted at Hizaeti Afras. The site is located near Wukro town, Tigray Regional State, in North Ethiopia. The main objective of the study was to test the suitability of the subsurface geological formations and structures for foundation of the proposed dam project based on the geo-electrical resistivity stratification of the site and magnetic anomalies obtained over the general area of the dam site. Hence different maps, models and curves including inverted 2D model section maps, apparent resistivity pseudo-depth section map, interpreted parameters of vertical electrical sounding curves, geo-electric section, magnetic anomaly map, analytical signal map, tilt derivative map, Euler depth solution map, 2D magnetic modeling and magnetic anomaly profile plots were developed using different mapping and interpretation software from the resistivity and magnetic data collected at field.

The interpretation of the stratifications observed on the 2D models is done using supporting information obtained from lithological well logging data and by correlating the models with magnetic anomaly profile plot.

Accordingly, the study area is interpreted to comprise of three layers in which the first layer is top soil which is composed of river sediments. This layer is thick in the eastern part of the study area however; its thickness gradually decreases as going west. Similarly the thickness of this layer decreases from north to south ranging from nine meter in the north to two meter in the south.

The second layer which is interpreted as weathered and fractured limestone with shale intercalation has considerable thickness in the western part of the study area as compared with the eastern part. The layer extends to a depth ranging from 21m in the south, downstream side, to 33m in the north, upstream side decreasing from north to south like that of the first layer.

The third layer, the black limestone, taken to be the bedrock in the area has undulating nature and depth to its surface is 33m in the western and northern parts of the study area and becomes shallower to about 15m towards the eastern and southern portions of the survey area.

Furthermore, the sliced stacked depth map and pseudodepth section map developed for dam site clearly show the vertical and horizontal apparent resistivity variation of the survey area. Accordingly the area is divided in to three distinct zones in which the first zone includes the western and northeastern part which is characterized by very low apparent resistivity values. This very low resistivity is the response of the water saturated weathered and fractured limestone. This zone goes to depths larger than 50m depth in the western part and it extends up to 35m depth in the northeastern part of the study area. Nevertheless, its lateral coverage decreases with depth in both areas. Therefore special attention should be given to the western and northeastern part of the study area in designing and implementation of the dam foundation.

The second zone comprises of the central part of the study area that exhibit intermediate apparent resistivity values. This area is interpreted as an area covered by weathered and fractured limestone with shale intercalation. This zone starts at about 10m depth but it increases its coverage laterally and in depth and extends to a depth beyond 50m. The shale unit which is intercalated with limestone can serve as water retaining unit and it can reduce liquefaction problems. Moreover it can be used as backfill material in itself for the foundation.

The third zone is the one which covers the southeastern part of the study area. These areas are described by very high apparent resistivity values which are the response of the black limestone formation. As it is indicated above, this formation is found at shallow depth in the southern and eastern parts of the study area. Similar to the second zone, this zone starts at about 10m depth in the southeast and increases its coverage laterally with depth towards north and west. The geo-electric section map shows the depth to this competent formation ranges from about 16m in the eastern part of the study area to 28m in the western part.

The analytical signal map and the tilt angle derivative map have clearly outlined the areas with high magnetic contrasts which indicated the presence of weak zones. A total of four aligned structures are depicted on these maps with different orientation. The orientations of the structures are dominantly N-S, NE-SW, NW-SE and E-W. Considering the current location of the proposed dam axis (which is oriented in the E-W direction), three of the structures can cut the dam axis at a near perpendicular direction and/or at high an angle. Especially the N-S trending structure existing at about 100m to 110m from the western flank of the dam axis runs nearly along the place where the existing dam failed. Therefore, it will be a threat for the new dam too if considerable measures are not taken.

Based on the interpretations made in this study, the areas described under zone three best fit for being dam foundation with some enhancements in design to prevent problems associated with the weak zones.

According to the design, the dam foundation will be constructed along Profile one (P-1). However from all the results of the applied geophysical methods in this work, this location is not preferable for the proposed dam foundation for the following reasons:-

- There is thick layer of top soil and weathered and fractured limestone which requires extensive earth works.
- In addition to the N-S trending structure, the other two structures with NE-SW and NW-SE orientation have a possibility of crossing the dam axis when extended. So that, they will negatively affect the dam foundation.
- It will require large finance to incorporate mechanism which will prevent seepage through the fractured limestone in the western side of the study area.
- It requires sophisticated engineering design to minimize the risk from the structures which will cross the dam axis.

Considering all these essential factors, it would be practical to prefarerably move the dam axis by about 150 m to downstream side.

6.2 Recommendations

Based on the results of this study, some important recommendations can be drawn as follows

- It will be better to move the site of dam foundation slightly (by about 150 m) to the downstream side.
- Careful consideration should be given to the weak zones mapped in the survey during designing the foundation.
- Excavation of weak material particularly in the western part must proceed as much as possible.
- Practically it is difficult to excavate 28m weak material therefore the design should include a blanketing material to prevent liquefaction and differential settlement.
- Foundation design should incorporate all necessary conditions to withstand any seismic hazard.
- To prevent all types of losses of water from the dam detailed and comprehensive investigation of the dam reservoir area should be made including seismic refraction.

REFERENCES

1. Anderson, N., Croxton, N., Hoover, R. and Sirles, P. (2008). Geophysical Methods Commonly Employed for Geotechical Site Characterization. Washington DC, p 2-21.
2. Asmelash Abay (2010). Presentation on Dam Failure Experience and its Implication to the Giba Dam. Mekelle University, Department of Earth Science, p 19-31.
3. Bell, F.G. (2007). Engineering Geology. 2nd Edition. Linacer House, Jordan Hill, Oxford, UK, p 353.
4. Beyth M. (1971). The Geology of Central and Western Tigray. Unpublished Report , EIGS, Addis Ababa pp .
5. Beyth M. (1972). A contribution to central and western Tigray. Report, Bonn. Company, Boston, pp 712.
6. Blakely R.J. (1995). Potential theory in Gravity and Magnetic applications. Cambridge University press, p 285-303.
7. Bommer, J. J. and Boore, M. D. (2004). Engineering Seismology. Encyclopedia of Geology, p 1-7.
8. Bossellini, A., Solomon Tadesse and Getaneh Assefa (1997). The Mesozoic Succession of The Mekell Outlier. Memo. Sci. Geol., **49;** 95-116.
9. Chambers, J.E., Oliver Kuras, Philip I.M, Richard D.O and Jonathan Hollands (2006). Electrical Resistivity Tomography Applied to Geologic, Hydrogeologic and Engineering Investigation at Former Waste Disposal Site. Geophysics, **7**; 231.
10. Dam Safety Committee (2010). General Dam Safety Considerations. available on http://www.damsafety.nsw.gov.au, p 6-7.
11. DeGroot-Hedlin, C. and Constable, S. (1990). Occam's Inversion to Generate Smooth, Two Dimensional Models form Magneto Telluric Data. Geophysics, **55**; 1613-1624.
12. Ethiopian Building Code Standard (1995). Code of Standards for Seismic Loads. Ministry of Work and Urban Development, Addis Ababa, Ethiopia.
13. Fang, H. and John, L.D. (2006). Introductory Geotechnical Engineering. New York, NY 10016, pp 545.
14. Fell, R., Patrick MacGregor, David Stapledon and Graeme Bell, (2005). Geothechnical Engineering of Dams. Taylor and Francis Group plc. London, UK, p 180-181.

15. Gebremedhin Berhane (2002). Geotechnical and Engineering Geological Investigation of Mekelle Area. MSc. Thesis (unpublished), Addis Ababa University, Addis Ababa, pp 163.
16. GETECH Group plc (2007). Advanced processing and interpretation of gravity and magnetic data, p 24-26. Retrived from www.getech.com.
17. Griffiths, D.H and Barker, R.D (1993). Two Dimensional Resistivity Imaging and Modelling in Areas of Complex Geology. Journal of Applied Geophysics, **29**; 211-226
18. Hailemariam Siyum (2011). Integrated Geophysical and Direct Geotechnical Investigation for Building Foundation. Masters Thesis, Addis Ababa University, Addis Ababa, pp 100.
19. Kearey, P., Michael Brooks and Lan Hill (2002). An Introduction to Geophysical Exploration. Third edition. Blackwell Science Ltd, UK, p 183-197.
20. Kirsch, R. (2009). Groundwater Geophysics. 2nd Edition. Hamburger Chaussee, Germany, p 275-286.
21. Loke, M.H (1999). Electrical Imaging Surveys for Environmental and Engineering Studies. A practical guide to 2-D and 3-D surveys. Penang, Malaysia, pp 57.
22. Lowrie, W. (2007). Fundamentals of Geophysics. 2nd Edition. Cambridge University, p 326.
23. McCann, D.M., Jackson, D.D. and Culshaw, M.G. (1987). The Use of Geophysical Methods in the Detection of Natural Cavities and Mineshafts. Journ. Eng. Geol. London, **20**; p 59-73.
24. McDowell, P .W, Dr Barker, R. D, Butcher, A.P, Dr Jackson P.D, Pro. McCann, D.M and Dr Sdipp, B.O (2002). Geophysics in Engineering Investigation. 6 Storey's Gate, Westminster, London, pp 249.
25. Midzi, V., Dumisani J.H., Lostina, S.C., Fekadu, K., Kuvvet, A., Daniel K.L., Gadi, T. and Fred, A.T. (1999). Seismic hazard assessment in Eastern and Southern Arical. Annali Di Gofisica, **42**; 1068-1072.
26. Miller, H.G. and V.Singh, (1994). Potential Field Tilt. A new concept for location of potential field source: Journal of Applied Geophysics, **32**; 213-217.
27. Milson, J. (2003). Field Geophysics. 3rd Edition. University College London, pp 249.
28. Reid, A. B., Allsop, J. M., Granser, H., Millet, A. J., and Somerton, I. W. (1990). Magnetic interpretation in 3D using Euler deconvolution. Geophysics, **55**; 80-91.
29. Reilly (1972). Use of International System of Units in Geophysical Publications. N.Z.J. Geol. Geophycis, **15**; 148-58.

30. Reynolds, J.M. (1997). An Introduction to Applied and Environmental Geophysics. John Wiley and Sons, Ltd, UK, pp 800.
31. Roest, W.R., Verhof, J. Pilkington, M. (1992). Magnetic interpretation using 3D analytic signal. Geophysics, **57**, 116-125.
32. Salem, A., Ravat, D., Gamey, T. J. and Ushijuma, K. (2002). Analytic signal approach and its applicability in environmental magnetic investigation. Journal of Appl. Geophysics, **49**; 231-244.
33. Sharma, P.V. (1986). Geophysical Methods in Geology. 2nd Edition. New York, pp 428.
34. Telford, W.M.**,** Geldart, L.P. and Sheriff, R.E. (1990). Applied Geophysics. *Second edition, p 522-539.*
35. Thompson, D.T. (1982). A new technique for making computer assisted depth estimates from magnetic data. Geophysics, **47**; 3-37.
36. Tigray Water resource, Mines and Energy Bureau (2011). Project of Extension and Repair of Hizaeti Afras Dam Site at Wukro Town. Tigray, Mekelle, pp 12.
37. Tigstu Haile (2010). Application of Electrical Resistivity Tomography. P 6. Retrieved from www.mawari.net.
38. Tilahun Mammo (2005). Site-specific ground motion simulation and seismic response analysis at the proposed bridge sites within the city of Addis Ababa, Ethiopia. Engineering Geology, **79**; 127-150.
39. U.S Army Corps of Engineers (2004). General Design and Construction Considerations for Earth and Rock Fill Dams, p 11. Retrieved from http://www.usace.army.mil/inet/usace-docs/.
40. U.S Department of the Interior (2001). Engineering Geology Field Manual. 2nd edition, p 29-30.

Appendix–1

Table 1 Structural indices for different geological structures (Reid et al., 1990).

Structural Index	Geological Structures
0	Contact
0.5	Thick Step
1	Sill/Dike
2	Vertical Pipe
3	Sphere

Appendix–2

Table 2 Lithological log of the borehole

No	Lithology	Dept (m)	
		From	To
1	Top soil (clay, silt, sand, and gravel with boulders)	0	9
2	Weathered and fractured limestone	9	18
3	Intercalation of shale and limestone	18	33
4	Black limestone	33	65
6	Light gray shale	66	72
7	Shale	72	75
8	Black limestone	75	78.5